Synthesis and Study of Imidazole-bearing Copper(I) Complexes and their Reversible Reaction with Dioxygen †

Connie L. Merrill and Lon J. Wilson *
Department of Chemistry, William Marsh Rice University, P.O. Box 1892, Houston, Texas 77251, U.S.A.
Thomas J. Thamann and Thomas M. Loehr
Department of Chemistry and Biochemical Sciences, Oregon Graduate Center, Beaverton, Oregon 97006, U.S.A.
Nancy S. Ferris and William H. Woodruff
Department of Chemistry, University of Texas at Austin, Austin, Texas 78712, U.S.A.

Magnetochemical and resonance-Raman spectroscopic measurements have been made on oxygenated solutions of {2,6-bis[1-(2-imidazol-4-ylethylimino)ethyl]pyridine}copper(I) cation and related complexes to characterize more fully the nature of the copper–dioxygen interaction. The role, if any, of the imidazole–nitrogen proton in the reversible oxygenation process has been examined. A possible correlation between the redox potential of the $Cu^{II} \rightleftharpoons Cu^{I}$ couple and the reaction of the copper(I) centre towards O_2 has been studied, and for completeness, copper(II) and zinc(II) analogues of all the copper(I) species have also been prepared and fully characterized. Although inconclusive in an absolute sense, the present studies are consistent with the oxygenation products of these copper(I) species being relatively stable $Cu-O_2$ or $Cu-O_2-Cu$ adducts, at least in the initial stages of oxygenation.

Recently we reported a copper(I) complex, $[CuL^1]^+$ (1), that reacts reversibly with dioxygen (O_2) under ambient conditions in solution, and suggested that such imidazole-bearing copper(I) species might serve as model compounds for the haemocyanin active site.[1] E.s.r. data at 100 K for the red deoxy- and green oxy-forms of the compound indicated that both were essentially diamagnetic. This result, combined with the O_2-uptake stoicheiometry of 1 O_2 per 2 Cu, suggested that the oxygenated copper complex may be binuclear, containing two copper(II) centres antiferromagnetically coupled through a peroxo-like bridge similar to that proposed for oxyhaemocyanin.[2] On the other hand, the $[CuL^3]^+$ cation (3) was found to undergo a much slower, non-stoicheiometric uptake of O_2,[1] indicating some irreversible oxidation of the copper(I) centre or perhaps the ligand framework itself. Thus, by varying the nature of the ligand, one can fine-tune the degree of reversible oxygenation within this class of copper(I) complex.

In a continuing study of these interesting copper(I) species, this work reports magnetochemical and resonance-Raman experiments on oxy- and deoxy-forms of (1) and (3) which have been conducted in order to characterize more fully the nature of the copper–dioxygen interaction. Also, four additional copper(I) derivatives, $[CuL^2]^+$ (2), $[CuL^4]^+$ (4), $[CuL^5]^+$ (5), and $[CuL^6]^+$ (6) have been synthesized in order to examine the role, if any, of the imidazole nitrogen proton of the $[CuL^1]^+$ species (1) in the reversible oxygenation process.§ Finally, for completeness and for comparison, copper(II) and zinc(II) complexes of all the quinquedentate ligands have been prepared and fully characterized by various spectroscopic and electrochemical methods.

Experimental

Materials.—All solvents were reagent grade, distilled before use, and stored over molecular sieves: CH_3OH from sodium metal, $(CH_3)_2SO$ from BaO, CH_3CN from $KMnO_4$ and Na_2CO_3, and CH_2Cl_2 from P_2O_5. Degassing was accomplished by the standard freeze–thaw method using Ar. Histamine free base [4-(2-aminoethyl)imidazole] was procured from Sigma Chemical Company; 2,6-diacetylpyridine, 2-(2-aminoethyl)-pyridine, α-chloro-*p*-xylene, and histamine dihydrochloride from Aldrich Chemicals; and $Cu[BF_4]_2 \cdot 6H_2O$, $Zn[BF_4]_2 \cdot 6H_2O$, Cu_2O, and $NaBF_4$ from Alfa Products. Electrochemical grade $NBu^n_4ClO_4$ and $NBu^n_4BF_4$ were purchased from G. Frederick Smith. Industrial grade N_2, Ar, and O_2 were obtained from Big Three Industries; N_2 and Ar were passed through H_2SO_4, then over solid KOH, a heated copper catalyst, and P_2O_5, and O_2 was purified by passing through H_2SO_4, then over solid KOH and Drierite.

Syntheses.—The copper(I) complexes were prepared under Ar using Schlenk glassware or under N_2 in a Vacuum/Atmospheres dry-box. The air-stable copper(II) and zinc(II) compounds were prepared in the open, but great care was taken to eliminate moisture from the solvents and glassware since their BF_4^- salts are hygroscopic. Chemical analyses were obtained commercially from Schwarzkopf Microanalytical Laboratory or at Rice University using a Perkin-Elmer 240C Elemental Analyzer.

N'-(p-Methylbenzyl)histamine, free base, was prepared by a modification of the method of Averill.[3]

Tetra(acetonitrile)copper(I) tetrafluoroborate, $[Cu(CH_3CN)_4][BF_4]$. This compound was prepared by the method of Hemmerich and Sigwart.[4] Copper(I) oxide (2.2 g) was added to a degassed mixture of water (40 cm^3) and CH_3CN (30 cm^3). Upon dropwise addition of $OEt_2 \cdot BF_3$ (60 cm^3), white needles formed. The mixture was then refluxed under Ar for 1 h. Upon cooling, the white needles were collected by filtration, dried *in vacuo*, and recrystallized from hot degassed CH_3CN. The purified product was dried *in vacuo* at room temperature, and stored under N_2.

{2,6-Bis[1-(2-imidazol-4-ylethylimino)ethyl]pyridine}zinc(II) tetrafluoroborate, $[ZnL^1][BF_4]_2$. A ligand solution was prepared by refluxing a CH_3OH solution (25 cm^3) of 2,6-diacetylpyridine (1 mmol) and histamine free base (2 mmol) for 1 h. This yellow solution, cooled to room temperature, was combined with solid $Zn[BF_4]_2 \cdot 6H_2O$ (1 mmol), and the mixture stirred at room temperature for 5 min. The resulting bright yellow solution was filtered and evaporated to dryness. The

† *Non-S.I. units employed:* atm = 101 325 Pa; G = 10^{-4} T; $\mu_B = 9.274 \times 10^{-24}$ J T^{-1}.

‡ Abstracted in part from the Ph.D. Dissertation of C. L. M., William Marsh Rice University, 1982.

§ *Note added in proof*: another copper(I) derivative of $[CuL^1]^+$ has recently been reported to react with dioxygen in a manner similar to $[CuL^1]^+$ (L. Casella, M. E. Silver, and J. A. Ibers, *Inorg. Chem.*, 1984, **23**, 1409.

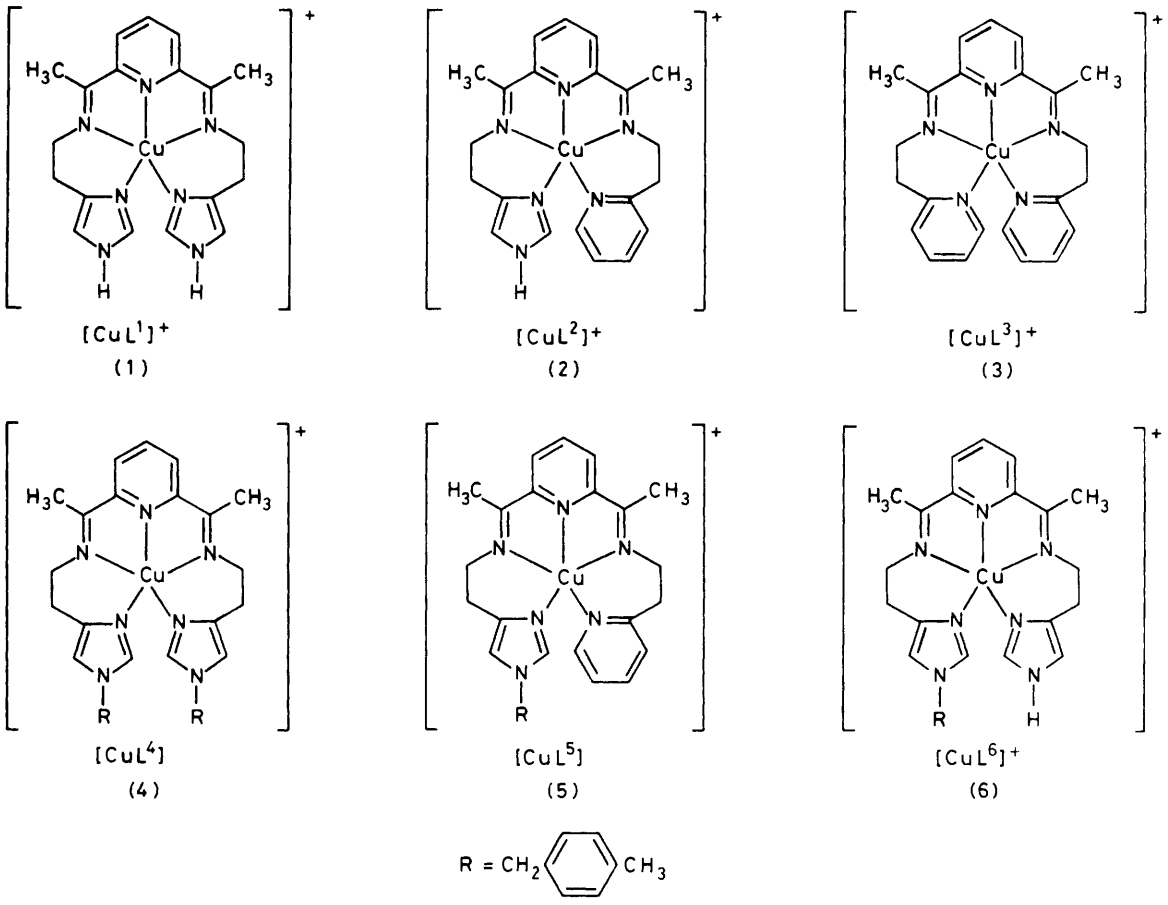

solid was recrystallized from CH_3OH–Et_2O (Found: C, 38.4; H, 4.0; N, 16.7. Calc. for $C_{19}H_{23}B_2F_8N_7Zn$: C, 38.8; H, 3.9; N, 16.7%). ^1H N.m.r. data for the perchlorate salt are reported in ref. 1*b*.

{2,6-*Bis*[1-(2-*pyridin*-2-*ylethylimino*)*ethyl*]*pyridine*}*zinc*(II) *tetrafluoroborate*, $[ZnL^3][BF_4]_2$. A ligand solution was prepared by heating a solution of 2,6-diacetylpyridine (1 mmol) and 2-(2-aminoethyl)pyridine (2 mmol) in CH_3OH (25 cm^3) under reflux for 1 h, after which it was cooled. Solid $Zn[BF_4]_2 \cdot 6H_2O$ (1 mmol) was then added. The resulting orange solution was stirred for *ca.* 5 min, filtered, and evaporated to dryness *in vacuo*. The orange solid was recrystallized from CH_3OH (Found: C, 45.0; H, 4.0; N, 11.5. Calc. for $C_{23}H_{25}B_2F_8N_5Zn$: C, 45.25; H, 4.1; N, 11.5%). ^1H N.m.r. data for the perchlorate salt are reported in ref. 1*b*.

{2,6-*Bis*[1-(2-N¹-p-*methylbenzylimidazol*-4-*ylethylimino*)-*ethyl*]*pyridine*}*zinc*(II) *tetrafluoroborate*, $[ZnL^4][BF_4]_2$. A ligand solution was prepared by heating a solution of 2,6-diacetylpyridine (1 mmol) and *N*¹-(*p*-methylbenzyl)histamine free base in CH_3OH (25 cm^3) under reflux for 1 h to yield a yellow solution. Upon cooling, this solution and solid $Zn[BF_4]_2 \cdot 6H_2O$ (1 mmol) were stirred for 5 min. The bright yellow-orange solution obtained was filtered and evaporated to dryness *in vacuo*. The resulting orange solid was recrystallized from a minimum amount of hot CH_3OH containing a small amount of Et_2O, to give a cream solid (Found: C, 52.8; H, 5.2; N, 12.35. Calc. for $C_{35}H_{39}B_2F_8N_7Zn$: C, 52.8; H, 4.9; N, 12.3%). ^1H N.m.r. (CD_3CN, $SiMe_4$ reference): δ 2.30 (s, 2 *p*-CH_3), 2.55 (s, 2 CH_3), 3.16 (t) and 3.94 (t) (4 CH_2), 5.04 (s, 2 CH_2), 6.95 (s, 2 imidazole H^5), 7.02 (s, 2 C_6H_4), 7.85 (s, 2 imidazole H^2), and 8.23 p.p.m. (m, 3 pyridine H). I.r. (Nujol): ν(C≡N) 1 585s ν(BF_4^-) 1 030 cm^{-1}.

{2-[1-(2-*Imidazol*-4-*ylethylimino*)*ethyl*]-6-[1-(2-*pyridin*-2-*ylethylimino*)*ethyl*]*pyridine*}*zinc*(II) *tetrafluoroborate monohydrate*, $[ZnL^2][BF_4]_2 \cdot H_2O$. A ligand solution was prepared by dissolving 2,6-diacetylpyridine (1 mmol) in dry CH_3OH (50 cm^3) and adding dropwise a solution of 2-(2-aminoethyl)-pyridine (1 mmol) and histamine free base (1 mmol) in CH_3OH (75 cm^3). During this procedure (*ca.* 45 min) the mixture was stirred and heated at 60 °C. Following the addition of the two bases, the ligand solution was allowed to reflux for another 45 min and then cooled to room temperature. To this yellow solution was added solid $Zn[BF_4]_2 \cdot 6H_2O$ (1 mmol), and upon stirring at room temperature the solution became deep orange. The solvent was removed *in vacuo* and the resulting orange solid crystallized from CH_3OH, yielding a slightly hygroscopic cream powder (Found: C, 40.9; H, 4.1; N, 13.7. Calc. for $C_{21}H_{26}B_2F_8N_6OZn$: C, 40.8; H, 4.25; N, 13.6%). ^1H N.m.r. (CD_3CN, $SiMe_4$ reference): δ 2.50 (s) and 2.61 (s) (2 CH_3), 3.10 (t), 3.44 (t), and 4.08 (m) (4 CH_2), 6.98 (s, imidazole H^5), 7.3—8.0 (m) and 8.25 p.p.m. (m) (imidazole H^2 and 7 pyridine H). I.r. (Nujol): ν(O–H) 3 620m; ν(N–H) 3 350s; ν(C=N) 1 610s and 1 590s; ν(BF_4^-) *ca.* 1 070s cm^{-1}.

{2-[1-(2-N¹-p-*Methylbenzylimidazol*-4-*ylethylimino*)*ethyl*]-6-[1-(2-*pyridin*-2-*ylethylimino*)*ethyl*]*pyridine*}*zinc*(II) *tetrafluoroborate monohydrate*, $[ZnL^5][BF_4]_2 \cdot H_2O$. The ligand was prepared by dissolving 2,6-diacetylpyridine (1 mmol) in dry CH_3OH (50 cm^3) and adding dropwise a solution of 2-(2-aminoethyl)pyridine (1 mmol) and *N*¹-(*p*-methylbenzyl)histamine free base (1 mmol) in CH_3OH (75 cm^3). During this addition, during *ca.* 45 min, the mixture was stirred and heated at 60 °C. The yellow ligand solution was then refluxed for 45 min and cooled to room temperature. Solid $Zn[BF_4]_2 \cdot$

$6H_2O$ (1 mmol) was added and the solution became bright yellow-orange. This solution was filtered and reduced to dryness *in vacuo*. Recrystallization of the resulting solid from CH_3OH–Et_2O produced a hygroscopic yellow powder (Found: C, 48.1; H, 4.8; N, 11.7. Calc. for $C_{29}H_{36}B_2F_8N_6OZn$: C, 48.3; H, 4.75; N, 11.65%). ^1H N.m.r. (CD_3CN, $SiMe_4$ reference): δ 2.28 (s, *p*-CH_3), 2.50 (s) and 2.56 (s) (2 CH_3), 3.07 (t), 3.43 (t), and 4.13 (m) (4 CH_2), 5.16 (s, CH_2), 7.10 (s, imidazole H^5), 7.15 (s, C_6H_4), 7.50—8.10 (m) and 8.25 (m) p.p.m. (imidazole H^2 and 7 pyridine H); see also Figure 1. I.r. (Nujol): ν(O–H) 3 610m; ν(C=N) 1 610s and 1 580s cm^{-1}; ν(BF_4^-) *ca.* 1 055s cm^{-1}.

{2-[1-(2-*Imidazol*-4-*ylethylimino*)*ethyl*]-6-[1-(2-N^1-p-*methylbenzylimidazol*-4-*ylethylimino*)*ethyl*]*pyridine*}*zinc*(II) *tetrafluoroborate dihydrate*, [ZnL^6][BF_4]$_2$·$2H_2O$. The ligand and the complex were prepared by the reaction of 2,6-diacetylpyridine (1 mmol) with a solution in CH_3OH of histamine free base (1 mmol) and N^1-(*p*-methylbenzyl)histamine free base (1 mmol), in a manner identical to that employed in the syntheses of the other zinc(II) hybrid-ligand compounds. Owing to the hygroscopic nature of this complex, normal recrystallization techniques were not successful. Rather, the yellow solid was first dissolved in hot, dry CH_3OH–Et_2O. Addition of dry Et_2O caused a deep orange oil to separate, leaving a yellow-orange mother-liquor. This solution was decanted from the oil, filtered, and reduced to dryness *in vacuo*. The resulting pale orange solid was very hygroscopic (Found: C, 45.1; H, 4.6; N, 13.35. Calc. for $C_{27}H_{35}B_2F_8N_7O_2Zn$: C, 44.5; H, 4.8; N, 13.5%). ^1H N.m.r. (CD_3CN, $SiMe_4$ reference): δ 2.21 (s, *p*-CH_3), 2.48 (s, 2 CH_3), 3.08 (t) and 3.85 (t) (4 CH_3), 5.04 (s, CH_2), 7.08br (s, 2 imidazole H^5 and C_6H_4), 7.87 (s) and 8.02 (s) (2 imidazole H^2), and 8.25 p.p.m. (m, 3 pyridine H). I.r. (Nujol): ν(O–H) 3 600m; ν(N–H) 3 320s; ν(C=N) 1 580s; ν(BF_4^-) *ca.* 1 050s cm^{-1}.

{2,6-*Bis*[1-(2-*imidazol*-4-*ylethylimino*)*ethyl*]*pyridine*}-*copper*(II) *tetrafluoroborate*, [CuL^1][BF_4]$_2$. The compound was prepared in the same manner as described for the zinc(II) complex, but using Cu[BF_4]$_2$·$6H_2O$. The recrystallized pale green solid showed $\mu_{eff.}$(solid, 298 K) 2.0 μ_B (Found: C, 39.3; H, 4.0; N, 16.6. Calc. for $C_{19}H_{23}B_2CuF_8N_7$: C, 38.9; H, 3.95; N, 16.7%). Electronic spectral data for the perchlorate salt are reported in ref. 1*b*.

{2,6-*Bis*[1-(2-*pyridin*-2-*ylethylimino*)*ethyl*]*pyridine*}*copper*-(II) *tetrafluoroborate*, [CuL^3][BF_4]$_2$. This compound was synthesized in the same manner as described for the zinc(II) complex, but using Cu[BF_4]$_2$·$6H_2O$. The recrystallized blue-green solid showed $\mu_{eff.}$(solid, 298 K) 2.1 μ_B (Found: C, 44.9; H, 4.3; N, 12.0. Calc. for $C_{23}H_{25}B_2CuF_8N_5$: C, 45.4; H, 4.1; N, 11.5%). Electronic spectral data for the perchlorate salt are reported in ref. 1*b*.

{2,6-*Bis*[1-(2-N^1-p-*methylbenzylimidazol*-4-*ylethylimino*)-*ethyl*]*pyridine*}*copper*(II) *tetrafluoroborate dihydrate*, [CuL^4]-[BF_4]$_2$·$2H_2O$. This compound was prepared in the same manner as described for the zinc(II) complex, but using Cu[BF_4]$_2$·$6H_2O$. The recrystallized lime green powder was fairly hygroscopic: $\mu_{eff.}$(solid, 298 K) 2.2 μ_B (Found: C, 50.45; H, 4.9; N, 11.4. Calc. for $C_{35}H_{43}B_2CuF_8N_7O_2$: C, 50.6; H, 5.2; N, 11.8%). U.v.–visible (CH_3CN), $\lambda_{max.}$/nm ($\varepsilon_{max.}$ dm^3 mol^{-1} cm^{-1}): 800 (120), 670 (136), 300 (br) (3.6×10^3), and 215 (3.5×10^4). I.r. (Nujol): ν(C=N) 1 585s; ν(BF_4^-) *ca.* 1 040s cm^{-1}.

{2-[1-(2-*Imidazol*-4-*ylethylimino*)*ethyl*]-6-[1-(2-*pyridin*-2-*ylethylimino*)*ethyl*]*pyridine*}*copper*(II) *tetrafluoroborate*, [CuL^2]-[BF_4]$_2$. This compound was prepared in the same manner as described for the zinc(II) complex, but using Cu[BF_4]$_2$·$6H_2O$. The recrystallized aquamarine coloured powder showed $\mu_{eff.}$ (solid, 298 K) 2.0 μ_B (Found: C, 42.4; H, 4.1; N, 13.8. Calc. for $C_{21}H_{24}B_2CuF_8N_6$: C, 42.2; H, 4.1; N, 14.1%). U.v.–visible (CH_3CN), $\lambda_{max.}$/nm ($\varepsilon_{max.}$/dm^3 mol^{-1} cm^{-1}): 780 (130), 675 (145), 300(br) (3.35×10^3), and 215 (3.15×10^4). I.r. (Nujol): ν(N–H) 3 320s; ν(C=N) 1 610 and 1 590s; ν(BF_4^-) *ca.* 1 080s cm^{-1}.

{2-[1-(2-N^1-p-*Methylbenzylimidazol*-4-*ylethylimino*)*ethyl*]-6-[1-(2-*pyridin*-2-*ylethylimino*)*ethyl*]*pyridine*}*copper*(II) *tetrafluoroborate monohydrate*, [CuL^5][BF_4]$_2$·H_2O. This compound was synthesized in the same manner as described for the zinc(II) complex, but using Cu[BF_4]$_2$·$6H_2O$. Recrystallization produced a blue-green powder: $\mu_{eff.}$ (solid, 298 K) 1.9 μ_B (Found: C, 48.8; H, 4.8; N, 11.9. Calc. for $C_{29}H_{36}B_2CuF_8N_6O$: C, 48.4; H, 4.8; N, 11.7%); u.v.–visible (CH_3CN) $\lambda_{max.}$/nm ($\varepsilon_{max.}$/dm^3 mol^{-1} cm^{-1}): 800 (139), 675 (154), 300 (br) (3.5×10^3), and 215 (3.5×10^4). I.r. (Nujol): ν(O–H) 3 620w; ν(C=N) 1 605 and 1 585s; ν(BF_4^-) *ca.* 1 055s cm^{-1}.

{2-[1-(2-*Imidazol*-4-*ylethylimino*)*ethyl*]-6-[1-(2-N^1-p-*methylbenzylimidazol*-4-*ylethylimino*)*ethyl*]*pyridine*}*copper*(II) *tetrafluoroborate dihydrate*, [CuL^6][BF_4]$_2$·$2H_2O$. This compound was prepared in the same manner as described for the zinc(II) complex, but using Cu[BF_4]$_2$·$6H_2O$. The resulting green solid product was hygroscopic: $\mu_{eff.}$(solid, 298 K) 1.8 μ_B (Found: C, 44.0; H, 4.6; N, 13.35. Calc. for $C_{27}H_{35}B_2CuF_8N_7O_2$: C, 44.6; H, 4.85; N, 13.5%). U.v.–visible (CH_3CN), $\lambda_{max.}$/nm ($\varepsilon_{max.}$/dm^3 mol^{-1} cm^{-1}): 800 (98), 670 (126), 300 (br) (3.2×10^3), and 215 (3.4×10^4). I.r. (Nujol): ν(O–H) 3 620m; ν(N–H) 3 315s; ν(C=N) 1 585s; ν(BF_4^-) *ca.* 1 040s cm^{-1}.

{2,6-*Bis*[1-(2-*imidazol*-4-*ylethylimino*)*ethyl*]*pyridine*}-*copper*(I) *tetrafluoroborate–water* (2/3), [CuL^1][BF_4]·$1.5H_2O$. This compound was prepared by the method of Simmons *et al.*[1b] A solution of 2,6-diacetylpyridine (1 mmol) and histamine free base (1 mmol) in degassed CH_3OH (26 cm^3) was refluxed for 1 h to yield a yellow solution, into which [Cu-(CH_3CN)$_4$]BF_4 (1 mmol) in degassed CH_3CN (20 cm^3) was syringed, immediately producing a deep red solution. This solution was evaporated to dryness *in vacuo* to yield a dark red solid, which was slightly hygroscopic: $\mu_{eff.}$(solid, 298 K) 0.8 μ_B (Found: C, 43.2; H, 4.5; N, 18.7. Calc. for $C_{19}H_{23}B$-CuF_4N_7·$1.5H_2O$: C, 43.3; H, 5.0; N, 18.6%). Electronic spectral data for the perchlorate are reported in ref. 1*b*.

{2,6-*Bis*[1-(2-*pyridin*-2-*ylethylimino*)*ethyl*]*pyridine*}*copper*-(I) *tetrafluoroborate–water* (1/2), [CuL^3]BF_4·$0.5H_2O$. This complex was synthesized by the method of Simmons *et al.*[1b] 2-(2-Aminoethyl)pyridine (2 mmol) was added dropwise to a solution of 2,6-diacetylpyridine (1 mmol) in CH_3OH (25 cm^3). This solution was then stirred and refluxed for *ca.* 1 h; it was then yellow. A solution of [$Cu(CH_3CN)_4$]BF_4 (1 mmol) in degassed CH_3CN (20 cm^3) was added by syringe, and the red solution obtained reduced to dryness *in vacuo*. Recrystallization from dry CH_3OH produced a red powder: $\mu_{eff.}$ (solid, 298 K) 0.2 μ_B (Found: C, 52.35; H, 4.8; N, 13.3. Calc. for $C_{23}H_{25}BF_4N_5$·$0.5\ H_2O$: C, 52.0; H, 4.9; N, 13.2%). ^1H N.m.r. and electronic spectral data for the perchlorate are reported in ref. 1*b*.

{2,6-*Bis*[1-(2-N^1-p-*methylbenzylimidazol*-4-*ylethylimino*)-*ethyl*]*pyridine*}*copper*(I) *tetrafluoroborate*, [CuL^4]BF_4. A solution of 2,6-diacetylpyridine (1 mmol) and N^1-(*p*-methylbenzyl)histamine free base (2 mmol) in degassed CH_3OH (25 cm^3) was refluxed for 1 h to yield a yellow solution. The salt [$Cu(CH_3CN)_4$]BF_4 (1 mmol) in degassed CH_3CN (20 cm^3) was then added by syringe, immediately producing a dark purple solution. Evaporation to dryness *in vacuo* yielded a purple-red hygroscopic solid: $\mu_{eff.}$(solid, 298 K) 0.8 μ_B (Found: C, 59.8; H, 5.7; N, 14.1. Calc. for $C_{35}H_{39}BCuF_4N_7$: C, 59.4; H, 5.55; N, 13.85%). U.v.–visible [$(CH_3)_2SO$], $\lambda_{max.}$/nm ($\varepsilon_{max.}$/dm^3 mol^{-1} cm^{-1}): 515 (1.8×10^3), 420 (1.76×10^3), and 310(sh) (3.3×10^3). I.r. (Nujol): ν(C=N) 1 580s; ν(BF_4^-) *ca.* 1 050s cm^{-1}.

{2-[1-(2-*Imidazol*-4-*ylethylimino*)*ethyl*]-6-[1-(2-*pyridin*-2-*ylethylimino*)*ethyl*]*pyridine*}*copper*(I) *tetrafluoroborate monohydrate*, [CuL^2]BF_4·H_2O. This compound was prepared by

controlled-potential electrolysis of the analogous copper(II) compound. Typically, the copper(II) complex (0.20 g) was electrolysed under nitrogen in a solution of CH_3CN with $NaBF_4$ (0.01 mol dm^{-3}) as supporting electrolyte at a potential of −0.55 V (*vs.* saturated calomel electrode, s.c.e.) for 2—3 h, when the current flow was effectively zero. The resulting red solution was reduced to dryness *in vacuo* in a Schlenk apparatus. The desired copper(I) compound was separated from the supporting electrolyte by dissolution in CH_2Cl_2. The CH_2Cl_2 filtrates were reduced to dryness *in vacuo* to yield a hygroscopic dark red product: $\mu_{eff.}$(solid, 298 K) 0.5 μ_B (Found: C, 47.4; H, 4.8; N, 15.3. Calc. for $C_{21}H_{26}BCuF_4N_6O$: C, 47.7; H, 5.0; N, 15.9%). U.v.–visible [$(CH_3)_2SO$], $\lambda_{max.}$/nm ($\varepsilon_{max.}$/dm^3 mol^{-1} cm^{-1}): 485 (2.0×10^3), 340 (3.55×10^3), and 290 (6.15×10^3). I.r. (Nujol): ν(O–H) 3 610m; ν(N–H) 3 320s; ν(C=N) 1 595 and 1 580s; ν(BF_4^-) *ca.* 1 070s cm^{-1}.

{2-[1-(2-N¹-p-*Methylbenzylimidazol*-4-*ylethylimino*)*ethyl*]-6-[1-(2-*pyridin*-2-*ylethylimino*)*ethyl*]*pyridine*}*copper*(I) *tetrafluoroborate trihydrate*, $[CuL^5]BF_4 \cdot 3H_2O$. This complex was prepared by controlled-potential electrolysis of the corresponding copper(II) compound. Typically, the copper(II) compound (0.1—0.2 g) was electrolysed at a potential of −0.55 V (*vs.* s.c.e.) for *ca.* 3 h, as in the preceding preparation. The resulting deep red solution was evaporated to dryness *in vacuo*. The solid, containing $NaBF_4$ and the desired copper(I) product, was extracted into degassed, dry CH_2Cl_2, and the filtrate dried *in vacuo* to yield the dark red copper(I) compound: $\mu_{eff.}$(solid, 298 K) 0.8 μ_B (Found: C, 51.9; H, 5.4; N, 12.2. Calc. for $C_{29}H_{40}BCuF_4N_6O_3$: C, 52.1; H, 5.7; N, 12.6%). U.v.–visible [$(CH_3)_2SO$], $\lambda_{max.}$/nm ($\varepsilon_{max.}$/dm^3 mol^{-1} cm^{-1}): 480 (1.24×10^3) and 320(sh) (3.0×10^3). I.r. (Nujol): ν(O–H) 3 620m; ν(C=N) 1 600 and 1 580s; ν(BF_4^-) *ca.* 1 055s cm^{-1}.

{2-[1-(2-*Imidazol*-4-*ylethylimino*)*ethyl*]-6-[1-(2-N¹-p-*methylbenzylimidazol*-4-*ylethylimino*)*ethyl*]*pyridine*}*copper*(I) *tetrafluoroborate dihydrate*, $[CuL^6]BF_4 \cdot 2H_2O$. This compound was prepared by controlled-potential electrolysis of the analogous copper(II) complex, by the procedure in the preceding preparations, at a potential of −0.575 V (*vs.* s.c.e.). The red-purple solid obtained was hygroscopic: $\mu_{eff.}$(solid, 298 K) 0.7 μ_B (Found: C, 44.05; H, 4.95; N, 13.1. Calc. for $C_{27}H_{35}BCuF_4N_7O_2$: C, 44.6; H, 4.85; N, 13.5%). U.v.–visible [$(CH_3)_2SO$], $\lambda_{max.}$/nm ($\varepsilon_{max.}$/dm^3 mol^{-1} cm^{-1}): 520 (2.25×10^3). I.r. (Nujol): ν(O–H) 3 610m; ν(N–H) 3 320s; ν(C=N) 1 580s; ν(BF_4^-) *ca.* 1 050s cm^{-1}.

Physical and Spectroscopic Measurements.—Solid-state i.r. spectra were recorded for Nujol mulls using NaCl plates and a Beckman IR-4230 spectrophotometer. The copper(II) and zinc(II) samples were prepared in air, while the copper(I) samples were mulled under N_2. U.v.–visible spectra were obtained on a Cary 17 recording spectrophotometer. The O_2-sensitive copper(I) samples were prepared on an Ar Schlenk line, using degassed CH_3CN or $(CH_3)_2SO$ as solvents, and sealed under Ar in the quartz cells for study. ^1H N.m.r. spectra were recorded at 90 MHz on a Varian EM390 spectrometer.

Warburg manometry was employed to measure oxygen uptake by the copper(I) complexes in solution at 23 °C [5] using a Precision Scientific (model 66662) manometer. Flask constants were determined using mercury. Typically, 30—40 mg of the copper(I) solid sample were weighed into the side arm of the flask and degassed $(CH_3)_2SO$ (3 cm^3) was syringed into the flask bottom. After equilibration to constant temperature under flowing dry N_2, the manometer was flushed with dry O_2 for 1 min, adjusted to atmospheric pressure, and tilted so as to dissolve the red copper(I) solid in the solvent. Complete O_2 uptake required *ca.* 15 min. A solvent blank was treated in the same manner, and its uptake volume subtracted from the uptake volume of the sample.

X-Band e.s.r. spectra were recorded at 100 K on a Varian E-line spectrometer; field positions were referenced relative to diphenylpicrylhydrazyl (dpph) and the detectable ($S = \frac{1}{2}$) copper(II) was determined quantitatively employing $CuSO_4$ samples of known concentration as the calibrant. The cycling procedure between deoxy/oxy/redeoxy states of the O_2-active copper(I) complexes involved cycling of the parent $(CH_3)_2SO$ solution; aliquots were taken at each stage and kept in e.s.r. tubes frozen at liquid-nitrogen temperature until the spectra were recorded.

Magnetic susceptibilities of the solids were measured by the Faraday technique using a Cahn model 6600-1 research magnetic susceptibility system and $Hg[Co(NCS)_4]$ as the calibrant. All measurements were made under 1 atm of He. Corrections for ligand and anion diamagnetism in all the copper complexes were made using the molar susceptibilities (c.g.s. units mol^{-1}) measured for the corresponding zinc(II) complexes: $[ZnL^1][BF_4]_2$, χ_M -2.980×10^{-4}; $[ZnL^3][BF_4]_2$, -1.702×10^{-4}; $[ZnL^4][BF_4]_2$, -1.084×10^{-4}; $[ZnL^2][BF_4]_2$, -3.539×10^{-4}; $[ZnL^5][BF_4]_2$, -5.386×10^{-4}; $[ZnL^6][BF_4]_2$, -1.355×10^{-4}.

The solution-state magnetochemical studies were also performed using the Cahn 6600 Faraday balance.[6,7] Using a quartz boat with a gas-tight cap, samples were sealed under a controlled environment to avoid contamination by moist air. The cryogenic apparatus consisted of an Air Products Interface model DMX-19 vacuum shroud, an LT-3-110 B Helitran system, and an APD-TL digital temperature readout monitoring an iron-doped gold *vs.* chromel thermocouple. The deoxy-$[CuL^1]^+$ samples were dissolved in degassed $(CH_3)_2SO$ and sealed for study under an Ar atmosphere. The oxy-$[CuL^1]^{n+}$ samples were prepared in $(CH_3)_2SO$, degassed with Ar, oxygenated with dry O_2, placed in a quartz boat, and sealed under O_2. All the samples were slowly cooled to liquid nitrogen temperature so as to freeze the solvent glass without cracking. Solutions of $[ZnL^1][BF_4]_2$ in $(CH_3)_2SO$ were studied under Ar and O_2 and used as blanks for the diamagnetic correction factors. The magnetochemical data (80—250 K) are reported (see below) as a 'difference' (χ_M *vs.* T^{-1}) plot depicting the net magnetic behaviour of the oxy-$[CuL^1]^+$ species in a frozen $(CH_3)_2SO$ glass.

Cyclic voltammetry measurements were recorded for solutions in CH_3CN under a constant flow of dry N_2 or O_2 using a PAR model 174 polarographic analyser. Electrolyses were carried out using a PAR polarographic model K62 cell. A three-electrode geometry with platinum buttons as the working and counter electrodes and a Fisher Scientific saturated calomel electrode (s.c.e.) as the reference electrode was employed. The reference electrode was separated from the bulk solution by a fritted-glass bridge containing supporting electrolyte solution, preventing aqueous contamination of the cell solution. Current–voltage curves were recorded on a Houston Instruments Omnigraphic 2000 *X–Y* recorder at scan rates of 200 and 500 mV s^{-1}. Differential pulse polarograms were obtained at a scan rate of 10 mV s^{-1} and a 0.5-s drop time. For the cyclic voltammetric and controlled-potential electrolytic experiments, 10^{-3} mol dm^{-3} solutions of the copper(II) samples in dry CH_3CN were used with $NBu^n_4ClO_4$, $NBu^n_4BF_4$, or $NaBF_4$ (0.1 mol dm^{-3}) as supporting electrolyte. Controlled-potential electrolytic syntheses were performed in a glass cell equipped with adaptors for attachment to a Schlenk line. A platinum-gauze electrode served as the working electrode with platinum wire and s.c.e. as the counter and reference electrodes, respectively. The solutions were stirred by bubbling N_2 through them during the electrolyses. Electronic integration of the current *vs.* time curves was achieved by a PAR model 379 coulometer and displayed as coulombs *vs.* time. All redox potentials are reported *vs.* s.c.e. and are uncorrected for liquid-junction potentials.

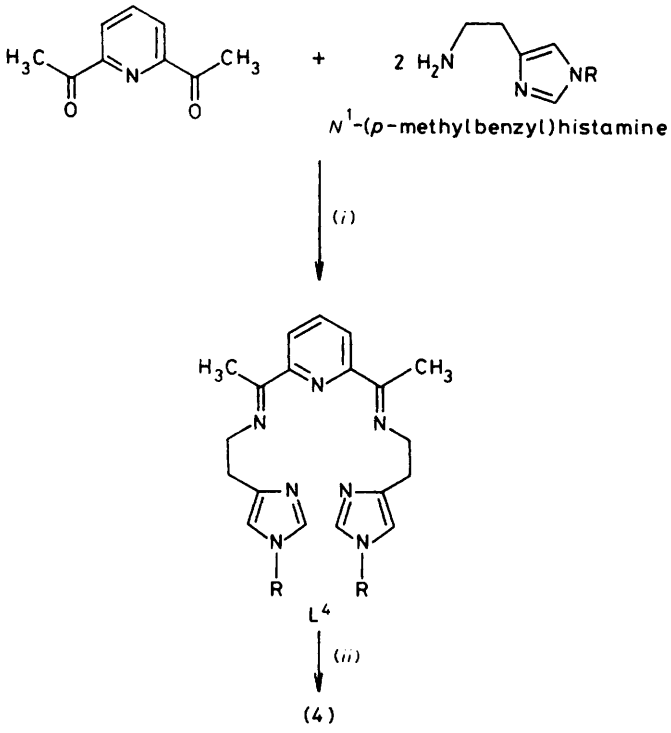

Scheme. Synthesis of {2,6-bis[1-(2-N^1-*p*-methylbenzylimidazol-4-ylethylimino)ethyl]pyridine}copper(I) tetrafluoroborate (R = CH_2-$C_6H_4CH_3$-*p*). (*i*) CH_3OH; (*ii*) CH_3CN, $[Cu(CH_3CN)_4]BF_4$

Resonance-Raman (r.R.) spectra obtained using visible excitation were recorded on a computerized Jarrell-Ash 25–300 Raman spectrophotometer as previously described.[8] The excitation wavelengths 457.9 and 514.5 nm were provided by a Coherent Radiation model 52MG Ar^+/Kr^+ laser. Plasma lines were eliminated by spike filters. A cooled ITT FW-130 (S-20) photomultiplier served as the scattered light detector and the output was processed in an ORTEC model 9302 Amplifier/Discriminator. Standard melting-point capillaries containing *ca.* 1 mm^3 of sample were inserted into a copper rod cold-finger immersed in liquid nitrogen and irradiated in a back-scattering geometry.[9] Laser power at the sample ranged from 10 to 50 mW, depending on the sample concentration (0.01—0.1 mol dm^{-3}).

Resonance-Raman spectra obtained using u.v. and violet excitation were recorded using a SPEX Ramlog EU spectrometer with a cooled RCA C31034A photomultiplier and an ORTEC 9300 series photon-counting system. Laser excitation at 413.1 and 406.7 nm was provided by a Spectra-Physics 171–01 krypton laser, and at 363.8 nm by an S-P 171-18 argon laser. Samples for room-temperature r.R. studies were contained in a spinning cell of the Shriver design.[10] The low-temperature experiments used frozen-solution samples cooled in liquid N_2 as described above.[9] Raman scattering was observed in a 135° back-scattering geometry in a plane perpendicular to the polarization of the laser beam. The following spectral acquisition conditions were the same for all samples and all excitation lines: scan speed, 0.5 cm^{-1} s^{-1} {except for oxy-$[CuL^1]^{n+}$, 0.2 cm^{-1} s^{-1}}; laser power at the sample, between 100 and 190 mW.

Results and Discussion

Synthesis and Characterization of the Complexes.—The complex $[CuL^4]BF_4$ (4) was synthesized by the route in the Scheme. The first step involves Schiff-base condensation of 2,6-diacetylpyridine and N^1-(*p*-methylbenzyl)histamine under Ar in refluxing methanol; addition of $[Cu(CH_3CN)_4]BF_4$ leads to a purple-red solution from which complex (4) may be isolated as a purple-red solid. While analytically pure copper(I) species (1), (3), and (4) have been prepared by this direct method, the hybrid-ligand compounds (2), (5), and (6) were best prepared by electrochemical reduction of their copper(II) analogues. The analogous zinc(II) and copper(II) compounds were all prepared on the open bench by the chemical method, using $Zn[BF_4]_2 \cdot 6H_2O$ or $Cu[BF_4]_2 \cdot 6H_2O$.

Pertinent i.r. data for all the complexes are in the Experimental section. In all cases, a C=N stretching frequency is observed in the 1 580—1 610 cm^{-1} region. The hybrid-ligand complexes, $[ML^2]^{n+}$ and $[ML^5]^{n+}$, possess two distinct C=N stretching frequencies, one near 1 580 and the other near 1 600 cm^{-1}. A second region of interest is 3 300—3 600 cm^{-1}. For the compounds possessing an unsubstituted imidazolyl moiety, a ν(N–H) stretch is observed at *ca.* 3 320 cm^{-1} whereas those complexes containing the *p*-methylbenzylimidazolyl unit are devoid of such absorptions. In general, the complexes which are hygroscopic also exhibit a ν(O–H) stretch at *ca.* 3 620 cm^{-1}. The B–F stretching frequency is quite broad, centred around 1 050 cm^{-1}, and is typical of compounds having BF_4^- counter ions.

Hydrogen-1 n.m.r. data for the $[ZnL^2]^{2+}$, $[ZnL^4]^{2+}$, $[ZnL^5]^{2+}$, and $[ZnL^6]^{2+}$ cations in CD_3CN are presented in the Experimental section and a typical spectrum for $[ZnL^5]^{2+}$ is shown in Figure 1. As in the cases of the $[ZnL^1]^{2+}$ and $[ZnL^3]^{2+}$ reported previously,[1b] there is no additional multiplicity in the spectra of any of the complexes, which might indicate the presence of an unco-ordinated ligand arm. Thus, the spectra support the proposal that all these complexes exist as five-co-ordinate species in solution, as is the case in the solid state for $[ZnL^1]^{2+}$ (and $[CuL^1]^{2+}$).[11] Attempts to prepare thoroughly deoxygenated copper(I) samples for characterization resulted only in ^1H n.m.r. spectra having severely broadened signals, apparently owing to the extreme O_2-sensitivity of the copper(I) complexes in general. ^1H N.m.r. spectra were not obtained for the copper(I) complexes, except for the relatively unreactive $[CuL^3]^+$ cation as reported earlier.[1b] The u.v.–visible spectra of all copper(II) complexes show at least two *d–d* bands in the 670—800 nm range. The positions and intensities of these bands (see Experimental section) are typical of copper(II) complexes. U.v.–visible data for the copper(I) complexes are also in the Experimental section, being dominated by a moderately intense charge-transfer band at *ca.* 480—520 nm, as well as a more intense band in the 290—340 nm region.

Reactivity of the Copper(I) Complexes with Dioxygen.—The oxygenation of the O_2-active copper(I) complexes is usually characterized by pronounced colour changes and the accompanying electronic spectral changes in the visible region. While red $[CuL^5]^+$ (5) ($\lambda_{max.}$ 480 nm, ε 1.24 × 10^3 dm^3 mol^{-1} cm^{-1}) does not undergo a colour change in the presence of O_2, * red solutions in CH_3CN or $(CH_3)_2SO$ of $[CuL^2]^+$, $[CuL^4]^+$, and $[CuL^6]^+$, (2), (4), and (6), respectively turn green upon exposure to dry O_2. The $[CuL^2]^+$ cation (2) ($\lambda_{max.}$ 485 nm, ε 2.0 × 10^3 dm^3 mol^{-1} cm^{-1}) clearly reacts with O_2, yet even with heating and prolonged purging with N_2, the khaki-green oxygenated solution remains green with no change in electronic spectrum [$\lambda_{max.}$(sh) *ca.* 430 nm], indicating that the oxygenation process is essentially non-reversible for this copper(I)

* *Note added in proof*: however, at least one preparation of $[CuL^5]BF_4$ did display a red ⟶ green colour change in the presence of O_2; the reason for this variation in reactivity with O_2 for the different preparations is not known.

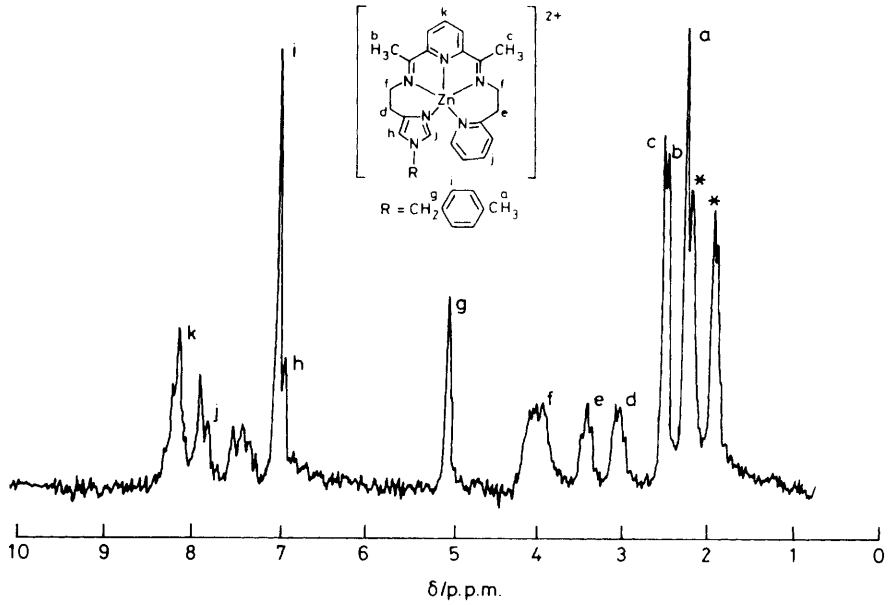

Figure 1. ^{1}H N.m.r. spectrum of $[ZnL^5][BF_4]_2$ in CD_3CN relative to internal $SiMe_4$

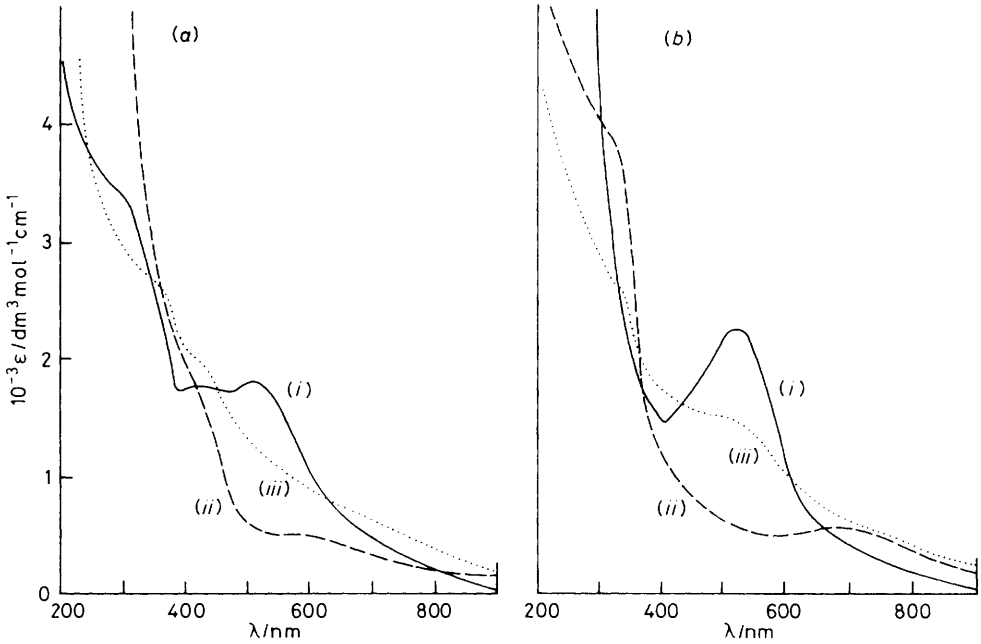

Figure 2. Electronic absorption spectra of (*a*) $[CuL^4]^+$ and (*b*) $[CuL^6]^+$ (0.5 mmol dm^{-3}) (*i*) in deoxygenated $(CH_3)_2SO$, (*ii*) solution (*i*) after oxygenation under O_2 (1 atm) with uptake of 0.5 mol of O_2 per Cu, and (*iii*) solution (*ii*) after deoxygenation by purging with N_2 and warming

hybrid-ligand complex. This result contrasts with that for the $[CuL^1]^+$ compound (1) where the red deoxy solution ($\lambda_{max.}$ 520 nm, ε 1.45 × 10^3 dm^3 mol^{-1} cm^{-1}) turns green in the presence of O_2 [$\lambda_{max.}$(sh.) *ca.* 410 nm] but reverts back to red upon warming and purging with N_2.[1b] As depicted in Figure 2(*a*), a red solution of deoxy-$[CuL^4]^+$ becomes pale green when O_2 is bubbled through it, but reverts to its red-orange colour on purging with N_2. While the degree of reversibility for this oxygenation process is lower than for $[CuL^1]^+$ (1), nevertheless some reversibility is evident. Finally, the oxygenation process for $[CuL^6]^+$ (6) is shown in Figure 2(*b*). Of the copper(I) complexes examined, the electronic spectral changes during a single oxy/deoxy cycle for this species most closely resemble those for the parent $[CuL^1]^+$ (1), and, from the spectral changes at 520 nm, the degree of reversibility is estimated to be *ca.* 65%, compared with *ca.* 85% for complex (1) at room temperature.[1b]

Warburg manometry has been employed to determine the stoicheiometry (O_2 : Cu molar ratio) of O_2 uptake by these copper(I) complexes in solution at room temperature. Paralleling $[CuL^3]^+$ (3), $[CuL^5]^+$ (5) is found not to react immediately with O_2 at 1 atm and 23 °C. However, upon standing under O_2 for an extended period (>1 h), the red copper(I) solution slowly becomes green-brown, indicating a slow, irreversible, chemical oxidation of some nature. One plausible explanation for the non-reactivity of the complex (5) involves the relative

Table 1. Cyclic voltammetric data for the BF_4^- salts under N_2 in CH_3CN at a scan rate of 200 mV s^{-1}

Complex	$E_{\frac{1}{2}}(Cu^{II} \rightleftharpoons Cu^{I})$ V *vs.* s.c.e.
$[CuL^3]^{2+}$	−0.20
$[CuL^5]^{2+}$	−0.25
$[CuL^2]^{2+}$	−0.27
$[CuL^4]^{2+}$	−0.32
$[CuL^6]^{2+}$	−0.33
$[CuL^1]^{2+}$	−0.35

stability of the copper(I) oxidation state in this ligand environment, as discussed below in the Electrochemistry section. On the other hand, oxygenation of the complexes (2), (4), and (6) is accomplished rapidly (10—12 min). It is noted that the rate of oxygenation is somewhat slower for the compounds (2) and (4) (time for complete oxygenation, *ca.* 20 min) than for (1) and (6) (*ca.* 10 min). Differences in the stability of the copper(I) centres toward oxidation and a possible difference in the mechanism for the oxygenation processes may account for this variation. As in the case of the parent complex (1), solutions of (2), (4), and (6) at 23 °C absorb 0.5 mol of O_2 per mol of copper. Thus, by varying the ligand environment, yet maintaining the presence of the imidazolyl moiety, the O_2 : Cu stoicheiometry has been firmly established as 1 : 2 for all the oxygenation processes.

Electrochemistry.—Electrochemical assays, including cyclic voltammetry in the presence and absence of dissolved O_2, have been performed to characterize the $Cu^{II} \rightleftharpoons Cu^{I}$ redox couple for each complex. Under N_2 the copper(II) species are characterized by nearly reversible, one-electron processes (confirmed by coulometry at potentials 250 mV cathodic of the $Cu^{II} \rightleftharpoons Cu^{I}$ couples) with the $E_{\frac{1}{2}}$ potentials being in the range −0.20 to −0.35 V *vs.* s.c.e. The $E_{\frac{1}{2}}$ values, as determined by differential pulse polarography, are in Table 1. In addition, cyclic voltammetry has been used to demonstrate the uniqueness and purity of the hybrid-ligand copper(II) complexes. For example, a physical mixture of $[CuL^1]^{2+}$ and $[CuL^3]^{2+}$ yielded two distinct cyclic voltammograms, whereas the hybrid-ligand complex $[CuL^2]^{2+}$ has a single wave with a half-wave potential between that of the di-imidazolyl and dipyridyl complexes $[CuL^1]^{+}$ and $[CuL^3]^{+}$ respectively (Figure 3). Likewise $[CuL^2]^{2+}$ exhibits an $E_{\frac{1}{2}}$ intermediate between that for the complexes $[CuL^4]^{2+}$ and $[CuL^3]^{2+}$. Since the redox potentials for $[CuL^1]^{2+}$ and $[CuL^4]^{2+}$ are so similar this electrochemical test for the distinctness of $[CuL^6]^{2+}$ is not clear-cut; nevertheless, elemental analyses (Experimental section) indicate the purity of this hybrid-ligand species as well. In addition to the copper(II) compounds, the analogous zinc(II) complexes have been examined electrochemically under N_2. Cyclic voltammograms for these zinc(II) species exhibit less reversible, one-electron reductions at potentials ranging from −1.12 to −1.40 V *vs.* s.c.e. Since these $E_{\frac{1}{2}}$ values are very negative and owing to the inherent stability of zinc(II) centres to reduction, these processes are undoubtedly ligand-centred reductions yielding ligand-based radical anions.

Cyclic voltammetry has also been employed to examine the oxygenation process of the copper(I) species as it is generated at the platinum electrode surface from its copper(II) analogue. Figure 4(*a*)—(*c*) illustrates such results for $[CuL^2]^{2+}$, $[CuL^4]^{2+}$, and $[CuL^6]^{2+}$. While all three species exhibit cyclic voltammograms unaffected by the presence of dissolved O_2 when the potential scan is uninterrupted, definite changes appear in the anodic wave if the potential is held cathodic of the $E_{\frac{1}{2}}$ value

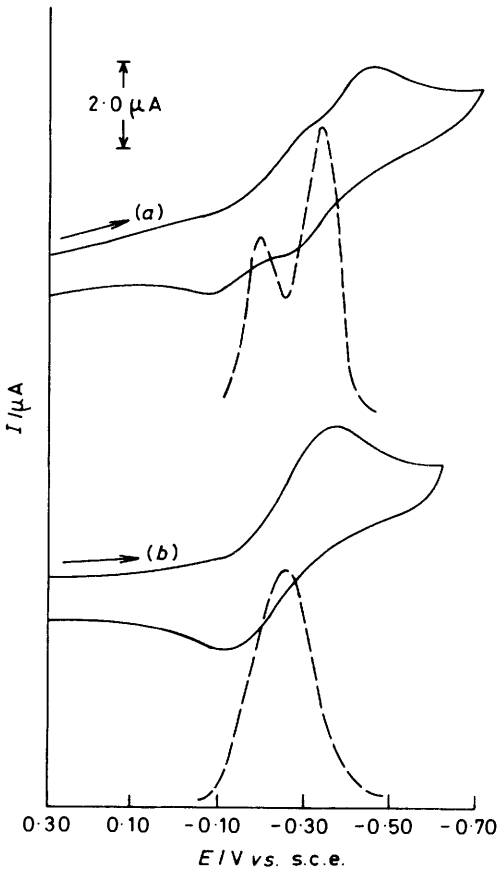

Figure 3. Cyclic voltammograms *vs.* s.c.e. and differential pulse polarograms for the copper(II) complexes (10^{-3} mmol dm^{-3}) in CH_3CN with $NBu^n_4ClO_4$ (0.1 mol dm^{-3}) at a scan rate of 200 mV s^{-1}. (*a*) A 1 : 1 mixture of $[CuL^1]^{2+}$ ($E_{\frac{1}{2}}$ −0.35 V) and $[CuL^3]^{2+}$ ($E_{\frac{1}{2}}$ −0.20 V); (*b*) $[CuL^2]^{2+}$ ($E_{\frac{1}{2}}$ −0.27 V)

for various time intervals. In the cases of $[CuL^2]^{2+}$ and $[CuL^4]^{2+}$, the anodic wave is greatly diminished but does not completely disappear, if the potential is held at −0.60 V for 9 and 25 s as shown in Figure 4(*a*) and (*b*). This result parallels the observation that the rate of O_2 uptake by these copper(I) complexes is qualitatively lower than for the parent $[CuL^1]^{+}$, where the anodic wave vanishes completely after a 9-s hold at −0.60 V.[1b] A subsequent scan, with no hold, yields the reversible cathodic and anodic waves, identical to the first scan under N_2. For $[CuL^6]^{2+}$ a similar result is obtained with the exception that a hold at −0.60 V for 25 s causes the anodic wave to disappear completely. The rescan with no hold, then produces the same cyclic voltammogram as that under N_2. The cyclic voltammogram of $[CuL^5]^{2+}$ in the presence of O_2 [Figure 4(*d*)] indicates that O_2 has no effect on the cyclic voltammogram when the potential is scanned, with no hold, cathodic of the $E_{\frac{1}{2}}$ value. Similarly, when the potential is held at −0.60 V for as long as 25 s, the cathodic and anodic waves appear as they do during scans under N_2 or O_2 with no hold. Thus, this hybrid-ligand copper(II) compound is similar to $[CuL^3]^{2+}$ in that no reaction between generated copper(I) and dissolved O_2 is observed electrochemically.

The data in Table 1 for the observed behaviour of the generated copper(I) derivatives under O_2 indicate that the more positive the $E_{\frac{1}{2}}$ the greater is the stability of the copper(I) species, generated at the electrode surface, and the slower is the reactivity of the copper(I) centre towards O_2 in a reversible

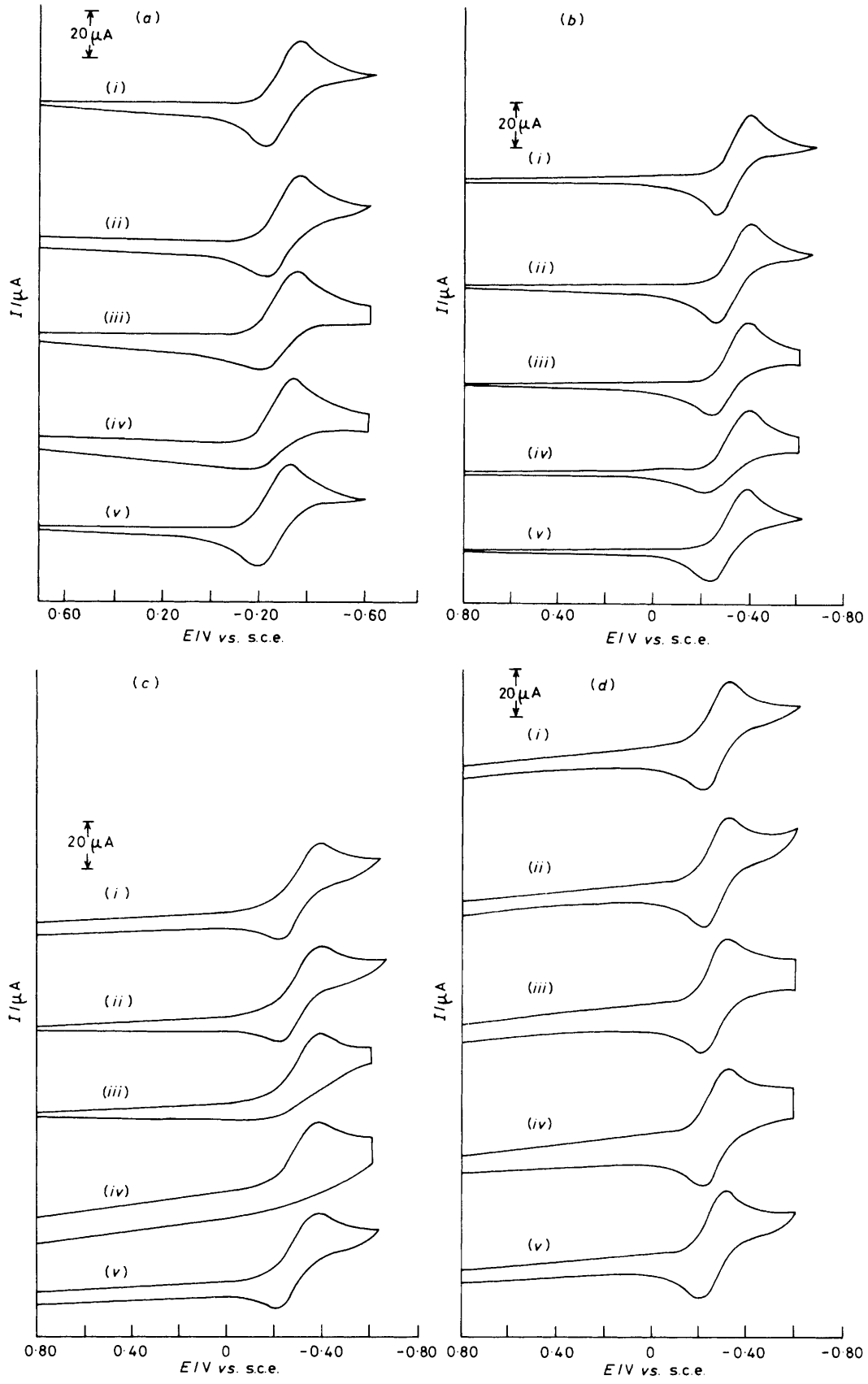

Figure 4. Cyclic voltammograms of the $Cu^{II} \rightleftharpoons Cu^{I}$ couple for the copper complexes (2.0 mmol dm^{-3}) in CH_3CN with $NBu^n_4ClO_4$ (0.1 mol dm^{-3}) at a 200 mV s^{-1} scan rate under the following conditions: (*i*) under N_2, (*ii*) under O_2, (*iii*) under O_2, holding at a potential of −0.60 V for 9 s, then scanning anodically, (*iv*) under O_2, holding at a potential of −0.60 V for 25 s, then scanning anodically, and (*v*) under N_2 again. (*a*) $[CuL^2]^{2+}$, (*b*) $[CuL^4]^{2+}$, (*c*) $[CuL^6]^{2+}$, and (*d*) $[CuL^5]^{2+}$

manner. The less reactive $[CuL^3]^+$ and $[CuL^5]^+$ species exhibit $E_{\frac{1}{2}}$ values of −0.20 and −0.25 V and the hybrid-ligand complex $[CuL^2]^+$ (which absorbs O_2 irreversibility) has an $E_{\frac{1}{2}}$ of −0.27 V. The $[CuL^4]^+$, $[CuL^6]^+$, and $[CuL^1]^+$ species, reacting with a progressively greater degree of reversibility towards O_2, have $E_{\frac{1}{2}}$ values of −0.32, −0.33, and −0.35 V, only 50—80 mV negative of that for $[CuL^2]^+$.

A correlation between copper(I) stability, the redox properties of the $Cu^{II} \rightleftharpoons Cu^{I}$ couple, and reactivity towards oxygenation or oxidation process has previously been noted.[12,13] Recently Gagné *et al.*[14] have synthesized some macrocyclic copper(I) complexes and have characterized the redox properties of these complexes in non-aqueous solution by cyclic voltammetry. These species exhibit $E_{\frac{1}{2}}$ values ranging from −0.46 to −0.80 V *vs.* s.c.e., or potentials much more negative than those of this work, and, as such, these species are much less stable with respect to a metal-centred oxygenation or oxidation. While Gagné's complexes react in solution with CO, the resulting Cu^{I}–CO adducts, in the presence of O_2, undergo irreversible oxidation to form μ-CO_3- and μ-OH-bridged copper(II) dimers.[14] On the other hand, $[CuL^1]^+$, and related derivatives, reacts reversibly in solution with O_2, yet does not react with CO under ambient conditions. From this admittedly brief comparative study the reactivity of these copper(I) co-ordination compounds towards CO and O_2 would appear to be mutually exclusive phenomena. It is probable that the copper(I) complexes of Gagné and co-workers with such negative $E_{\frac{1}{2}}$ values are in effect too reactive towards oxidation by O_2 to form stable Cu–O_2 adducts. In addition, molecular geometry changes that should occur during an oxidative addition involving O_2 may be important, and the relatively fixed structure of Gagné's macrocyclic compounds may be too rigid to allow the kinds of facile changes in co-ordination geometry that accompany an O_2-binding, oxidative addition process.

Relevant to O_2-active $[CuL^1]^+$, *X*-ray structural information is now available for the analogous copper(II) and zinc(II) complexes.[11] The five-co-ordinate $[ML^1]^{2+}$ (M = Cu^{II} or Zn^{II}] complexes are isomorphous and isostructural, with the co-ordination about copper(II) and zinc(II) describable as intermediate between an idealized trigonal bipyramid and a square pyramid. On the basis of this structural study it is possible to speculate on the structural nature of a simple O_2 adduct with $[CuL^1]^+$ and on the mechanism for reversible O_2 binding. While five-co-ordinate copper(I) species are still relatively rare, a few are now known,[15] and the predisposition of the five nitrogen-donor atoms of the L^1 ligand suggests that $[CuL^1]^+$ will ultimately prove to be five-co-ordinate as well. Assuming this to be the case, the most reasonable site for initial O_2 ligation appears to be *trans* to the pyridine-nitrogen atom and between the two imidazole rings. However, owing to steric hindrance with imidazole nitrogens, a bent O_2 ligated at this site would produce an O_2 adduct (probably more correctly written as Cu^{II}–O_2^-) which could gain no stabilization by *intramolecular* Cu–$O_2^- \cdots$ NH(imidazole) hydrogen-bonding interactions of the type shown to exist between end-on-bonded O_2 in (heme)Fe–O_2^- and the distal histidine-imidazole proton in oxymyoglobin.[16] On the other hand, the product of O_2 ligation could be a five-co-ordinate species obtained by release of an imidazole ligand from the copper co-ordination sphere at the time of attack by O_2. Such a species could then be stabilized by an NH $\cdots$ O hydrogen bond between the end-on-bonded O_2 ligand and the hydrogen atom of the 'free' imidazole. The resulting free space around the metal would be advantageous for formation of a binuclear copper species of the nature discussed below. Finally, an end-on-bonded configuration for O_2 is also suggested by the fact that the stoicheiometry of the reversible $2Cu^{I} + O_2 \rightleftharpoons$ oxy-product reactions implies that the final oxygenated materials are binuclear in copper, and an end-on-bonded peroxo-like bridge, *i.e.*, Cu^{II}–O_2^{2-}–Cu^{II}, would probably be necessary to span the distance (3—5 Å) required to bridge the two copper centres.

The disappearance of the anodic peak under an O_2 atmosphere is probably due to the reaction of O_2 with the electrochemically generated copper(I) centre. The reappearance of the anodic wave upon scanning with no hold indicates that the electrode surface is not contaminated with any oxidized products that would have prevented the observation of the anodic wave. With $[CuL^6]^{2+}$ behaving electrochemically most like the parent $[CuL^1]^{2+}$, these results are consistent with an electrode mechanism for the oxygen reaction as proposed previously [1b] for the oxygenation of $[CuL^1]^+$. In this mechanism the copper(II) complex is reduced under an O_2 atmosphere as the potential is scanned negative of the $E_{\frac{1}{2}}$ value. During the hold procedure, at −0.60 V, the electrochemically generated copper(I) reacts with dissolved O_2. This proposed oxidative-addition reaction, with the chemical binding of O_2 to two copper(I) centres to form a supposed μ-dioxygen species, would formally result in the metal centres being 'oxidized' and O_2 being 'reduced' to perhaps a peroxide anion. Accordingly, the oxy-form of this complex would then have a binuclear LCu^{II}–O_2^{2-}–$Cu^{II}L$ structure. Thus, as the potential scan is reversed toward the positive direction, there is no anodic wave because there is no available copper(I) species for oxidation.

As an alternative, the oxygenation process could involve some kind of imidazole-nitrogen 'proton-involvement' scheme whereby $[CuL^1]^+$ could react with O_2 to yield a μ-dioxygen species by the mechanism in reactions (i) and (ii). In such a

$$2[Cu^{I}L^1]^+ + O_2 \rightleftharpoons [(Cu^{II}L^1)_2(O_2^{2-})]^{2+} \quad \text{(i)}$$

$$[(Cu^{II}L^1)_2(O_2^{2-})]^{2+} \rightleftharpoons H_2O_2 + 2[Cu^{II}(L^1 - H)]^+ \quad \text{(ii)}$$

scheme, proton abstraction occurs to give, for example, H_2O_2 and a mono-deprotonated oxidized copper(II) product. In fact, a similar deprotonation mechanism has recently been proposed for the reaction of O_2 with tris(2,2′-bi-2-imidazoline)iron(II).[17] The final $[Cu^{II}(L^1 - H)]^+$ product would need to be dimerized or polymerized to explain the observed reduction in e.s.r. intensity (see below) of the oxy-product and the removal of O_2 would then have to cause spontaneous reduction to $[Cu^{I}L^1]^+$ to complete the reversible oxygenation cycle.

While both the above oxygenation mechanisms have merit with respect to $[CuL^1]^+$, the possibilities for $[CuL^4]^+$, $[CuL^5]^+$, and $[CuL^6]^+$ are, in general, more restricted. The $[CuL^5]^+$ complex contains no imidazole-nitrogen protons and it does not react with O_2 in a stoicheiometric, reversible fashion. Yet $[CuL^4]^+$ and $[CuL^6]^+$ do absorb O_2 (O_2 : Cu = 1 : 2), each at a rate similar to that of the parent $[CuL^1]^+$. Since the oxygenation of these copper(I) complexes in solution is partially reversed on purging with N_2, the O_2 reactivity profiles of $[CuL^4]^+$ and $[CuL^6]^+$ parallel that of the parent $[CuL^1]^+$. The hybrid-ligand complex $[CuL^2]^+$ seems to be on the borderline between a reversible and an irreversible oxidation process. This copper(I) complex reacts stoicheiometrically with O_2 (O_2 : Cu = 1 : 2), but at a much slower rate than the other active copper(I) species (1), (4), and (6), and the oxygenation process appears to be irreversible. Clearly, oxygenation of $[CuL^4]^+$ cannot involve an acidic imidazole-nitrogen proton. Possibly the oxygenation mechanisms for $[CuL^1]^+$ and $[CuL^4]^+$ differ, but this seems unlikely. Of course, the solvent [in this case $(CH_3)_2SO$ or CH_3CN] is also a potential source of protons, but the solubility properties of the

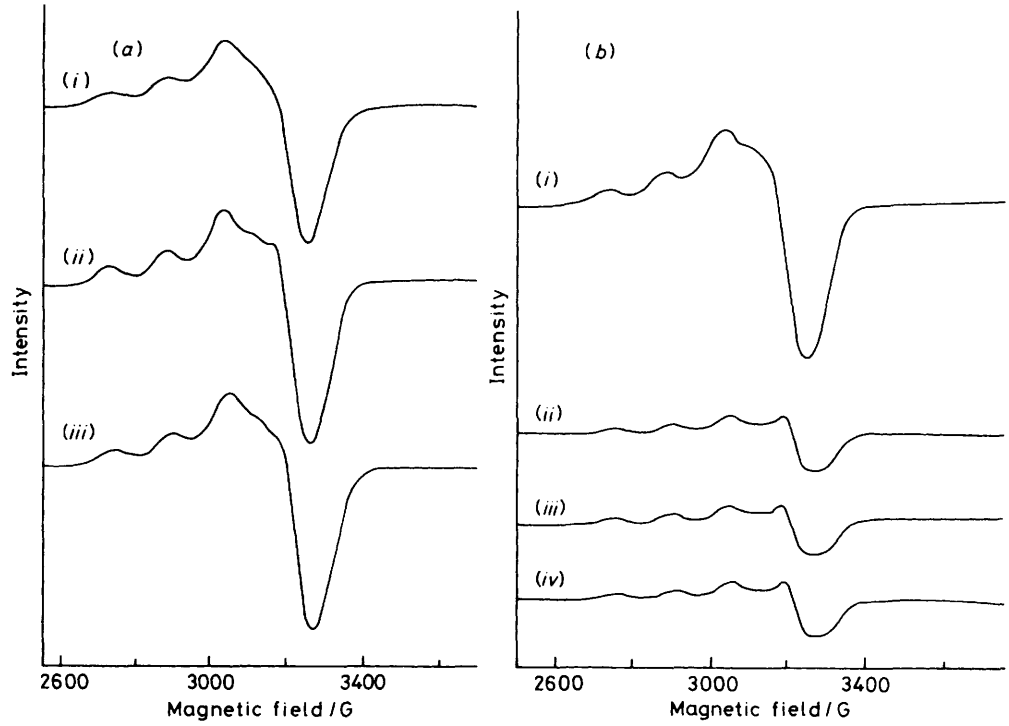

Figure 5. E.s.r. spectra for the copper(II) complexes (10^{-3} mmo /dm^{-3}) in $(CH_3)_2SO$ glasses at 100 K: (*i*) $[CuL^2]^{2+}$, (*ii*) $[CuL^4]^{2+}$, and (*iii*) $[CuL^5]^{2+}$. (*b*) E.s.r. spectra for the deoxy- and oxy-copper complexes (10^{-3} mmol dm^{-3}) in $(CH_3)_2SO$ glasses at 100 K: (*i*) $[CuL^6]^{2+}$ (actual intensity), (*ii*) $[CuL^6]^+$ (deoxy, 2× actual intensity), (*iii*) solution (*ii*) after absorption of 1 mol of O_2 per 2 mol of Cu (oxy, 2× actual intensity), and (*iv*) solution (*iii*) degassed with N_2 (redeoxy, 2× actual intensity)

copper(I) salts preclude the use of aprotic solvents to test whether such solvent involvement is important.

Finally, the reactivity of these copper(I) compounds towards O_2 could involve yet another, drastically different, possibility whereby the ligand framework itself is ultimately oxidized. The most likely site for such an oxidation would seem to be the imidazole moiety. While imidazoles are quite resistant to oxidation, drastic oxidation of methylbenzimidazole by concentrated potassium permanganate solution removes the benzene functional group with the formation of imidazole-4,5-dicarboxylic acid.[18] Subsequent decarboxylation, with heating, then yields the unsubstituted imidazole compound. A well documented mechanism involving the oxidation of the imidazole rings with O_2 might also be invoked to explain the observed reactivity of these copper(I) complexes towards O_2.[19-22] In the presence of sensitizers, such as Rose Bengal or Methylene Blue, and visible light, triplet O_2 is photosensitized to give singlet O_2, which then reacts in a concerted fashion with imidazoles to yield several photo-oxidized products, including endoperoxide intermediates.[19] While some substituted endoperoxides undergo a reverse Diels–Alder reaction at low temperature to regenerate some singlet O_2 and starting material, the majority of substituted endoperoxides form a complex mixture of products.[20] Unsubstituted imidazole indergoes a very slow photo-oxidation (requiring about 2 weeks), and the irradiation usually causes irreversible degradation. In addition, the oxygenation of histidine requires greater than 1 mol of O_2 per mol of substrate destroyed and yields several complex products.[21,22] In fact, this photo-oxidation procedure has been employed to elucidate structure–function relationships in the haemocyanins. In the photochemical irradiation of *Octopus vulgaris* haemocyanin, using various external photosensitizers, tryptophyl and histidyl side-chain residues are selectively photo-oxidized, forming endoperoxide-like intermediates and fluoresence emission spectra of the photo-oxidized protein indicate that in addition to histidine, a tryptophyl residue may be located near the copper–dioxygen binding site.[23] To consider the possibility of endoperoxide formation (perhaps catalysed by Cu^I) in the present oxygenation reaction, the oxygenation of $[CuL^1]^+$, $[CuL^4]^+$, $[CuL^6]^+$, and $[CuL^2]^+$ was also examined in the dark, but no noticeable difference in the red $\rightleftharpoons$ green oxygenation cycle was observed. Thus, the absence of light has no apparent effect on the present reversible oxygenation processes and an imidazole photo-oxidation reaction mechanism appears to be at best a remote possibility.

In summary, after considering both a ligand 'proton involvement' and an imidazole photo-oxidation mechanism as possibilities, available information still points toward simple adduct formation of O_2 with the present copper(I) complexes that react reversibly with O_2. In addition, the following e.s.r., magnetochemical, and resonance-Raman results can also be taken to imply that these copper(I) complexes serve as simple oxygen carriers with the oxy-form being binuclear in copper.

E.S.R. Spectroscopy.—E.s.r. spectral data obtained at 100 K for the present copper(II) complexes are typical of magnetically dilute $S = \frac{1}{2}$ centres with spectral characteristics resembling those of copper(II) in other five-co-ordinate geometries. For example, the $g_{\|}$, $g_{\perp}$, and $a_{\|}$ parameters from the data shown in Figure 5(*a*), and presented in Table 2 for three of the new copper(II) complexes, are similar to those obtained for two nearly square-pyramidal species $[Cu\{(Et_2NCH_2CH_2NEtCH_2)_2\}X]X$ (X = Cl, $g_{\|} = 2.22$, $g_{\perp} = 2.06$, $a_{\|} = 158$ G; X = Br, $g_{\|} = 2.22$, $g_{\perp} = 2.05$, $a_{\|} = 158$ G).[24]

Figure 5(*b*) shows the e.s.r. spectrum at 100 K of $[CuL^6]^{2+}$ which has nearly identical e.s.r. parameters to those of the other copper(II) complexes in Table 2. However, also shown in

Table 2. E.s.r. data for the copper complexes (10^{-3} mol dm^{-3}) as $(CH_3)_2SO$ glasses at 100 K

Compound	$g_{\parallel}$	$g_{\perp}$	$a_{\parallel}$/G
$[CuL^2]^{2+}$	2.21	2.07	155
$[CuL^4]^{2+}$	2.22	2.06	150
$[CuL^5]^{2+}$	2.21	2.06	155
$[CuL^6]^{2+}$	2.22	2.06	145
$[CuL^6]^{+}$ * (*ii*)	2.22	2.05	145
$[CuL^6]^{+}$ * (*iii*)	2.22	2.06	150
$[CuL^6]^{+}$ * (*iv*)	2.22	2.05	145

* (*ii*)–(*iv*) Refer to Figure 5(*b*); only 5—10% of available copper is detected as Cu^{II}.

Figure 5(*b*) are the e.s.r. spectra of the deoxy-, oxy-, and redeoxy-forms of $[CuL^6]^+$. The weak signals obtained for the deoxy- and oxy-forms of this copper(I) compound closely resemble those reported earlier [1b] for $[CuL^1]^+$ and probably arise from a small amount of copper(II) impurity since the e.s.r. spectra for the deoxy- and oxy-forms are essentially identical with little or no variation in signal intensity or multiplicity upon deoxy/oxy/redeoxy cycling. The deoxy-, oxy-, and redeoxy-forms of $[CuL^2]^+$ and $[CuL^4]^+$ also give spectra similar to those of Figure 5(*b*). Assuming that these weak e.s.r. signals (representing only 5—10% of the available copper in the sample) are due to copper(II) impurities or oxidation products, then the oxy-forms of these copper(I) complexes are, indeed, e.s.r.-silent as is oxy-$[CuL^1]^{n+}$.[1b] In this sense, the oxy-forms of these copper(I) complexes accurately mimic the e.s.r.-silent behaviour of oxyhaemocyanin where the active-site bridging structure is thought to be (A),[2b,25-32] and

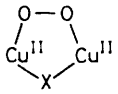

(A)

where the e.s.r. silence arises from a strong antiferromagnetic coupling interaction [$-J$(Cu–Cu) $\geqslant$ 550 cm^{-1}] between the copper(II) centres to give oxyhaemocyanin a resultant $S = 0$ ground state.[2] Variable-temperature magnetic susceptibility data reported below for oxy-$[CuL^1]^{n+}$ also strongly indicate that a Cu–Cu antiferromagnetic exchange interaction is responsible for the observed e.s.r. silence of the oxy-form of these synthetic copper(I) systems.

Magnetochemical Studies.—Variable-temperature (80—250 K) magnetic susceptibility measurements on an oxygenated solution of $[CuL^1]^+$ have been obtained to ascertain whether a Cu–Cu antiferromagnetic interaction might explain the e.s.r. silence of the oxy-derivative. The magnetochemical data are reported in Tables 3—5. The deoxy-$[CuL^1]^+$ sample, under Ar, exhibits a Curie-type behaviour (Table 3), reflecting the presence of a small amount of copper(II) impurity; this impurity, also observed in the e.s.r. spectrum of this complex (see above), provides a constant contribution to the overall paramagnetism of the sample, but does not adversely affect the determination of the magnetic susceptibility of oxy-$[CuL^1]^{n+}$. Variable-temperature magnetic susceptibility data for oxy-$[CuL^1]^{n+}$ (Table 4), $[ZnL^1]^{2+}$ under O_2, and $[ZnL^1]^{2+}$ under Ar (Tables 3 and 4) have also been obtained. Using the molar susceptibilities of the two zinc(II) preparations (constant over the full temperature range) as blanks and the molar susceptibility of the deoxy-$[CuL^1]^+$ sample to serve as a blank for any oxidized copper(II) impurities present, a 'difference'

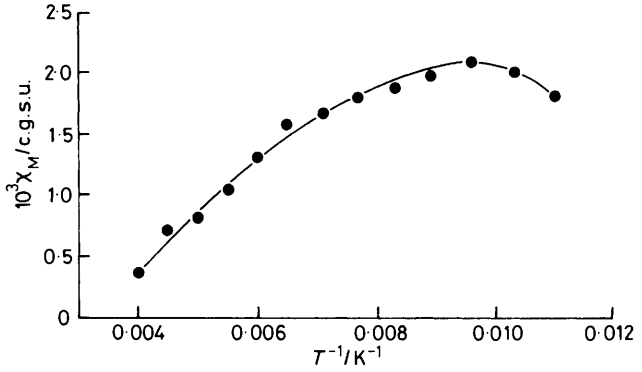

Figure 6. χ_M *vs.* T^{-1} 'difference' plot for oxy-$[CuL^1]^{n+}$ (0.1 mmol dm^{-3}) in $(CH_3)_2SO$ solution; T_N *ca.* 105 K

molar susceptibility for oxy-$[CuL^1]^{n+}$ (Table 5) can be calculated from equation (iii). The Neél temperature (T_N)

$$\chi_M(\text{difference}) = (\chi_M \text{ of oxy-}[CuL^1]^{n+} - \chi_M \text{ of } [ZnL^1]^{2+} \text{ in } O_2) - (\chi_M \text{ of deoxy-}[CuL^1]^{+} - \chi_M \text{ of } [ZnL^1]^{2+} \text{ in Ar}) \quad \text{(iii)}$$

for an antiferromagnetic exchange interaction is the temperature on a χ_M *vs.* T^{-1} plot where a change in slope occurs. As depicted in Figure 6, such a change occurs around 105 K for a frozen, oxygenated solution of Cu^I in Me_2SO, where the observed pattern is very typical of an antiferromagnetic interaction. None of the other samples [deoxy-Cu^I and the zinc(II) preparations] showed any evidence of such non-linear χ_M *vs.* T^{-1} plots.

Assuming that the magnetic behaviour for the oxy-$[CuL^1]^{n+}$ sample of Figure 6 arises from antiferromagnetic coupling between two copper(II) centres, the classical model for a two $S = \frac{1}{2}$ spin interaction, where $H = -2JS_1 \cdot S_2$ and $2J$ is the splitting between singlet and triplet energy levels, gives equation (iv). From this relationship, $-J$(Cu–Cu) for oxy-

$$-J/\text{cm}^{-1} = ca.\ \tfrac{2}{3}T_N/\text{K} \quad \text{(iv)}$$

$[CuL^1]^{n+}$ is *ca.* 70 cm^{-1}. Thus, this result indirectly provides further indication, that for oxy-$[CuL^1]^{n+}$, the copper centres may be pairwise linked by an O_2 bridge that fosters antiferromagnetic coupling of moderate magnitude. Of course, the exact magnitude of $-J$ depends on the geometrical relationship between the orbitals on the metals with unpaired electron density and the ligand orbitals through which the exchange interaction is fostered. Since this relationship is most probably different for oxyhaemocyanin and oxy-$[CuL^1]^{n+}$, a quantitative comparison between $-J$ for the protein and the present system cannot be made, especially since oxyhaemocyanin also seems to contain an endogenous bridge, possibly tyrosine.[28-32] However, the present magnetochemical study qualitatively indicates that the copper centres in the oxy-$[CuL^1]^+$ sample are indeed antiferromagnetically coupled, and that coupling of a moderate magnitude ($-J$ = *ca.* 70 cm^{-1}) can manifest itself in the form of e.s.r. silence.

Resonance-Raman Studies.—The vibrational stretching frequencies [ν(O–O)] for oxygen and its various reduced states are well known: O_2, 1 556; O_2^- (superoxide), 1 145; and O_2^{2-} (peroxide), 770 cm^{-1}.[33] Comparison between these values and ν(O-O) observed for oxyhaemoglobin (1 107 cm^{-1}) and the oxy-'picket fence' porphyrin complex (1 160 cm^{-1}) has led to an Fe^{III}–O_2^- formalism for the metal–oxygen bonding in these iron-based oxygen carriers.[34] Furthermore, *X*-ray struc-

Table 3. Magnetochemical data for deoxy-$[CuL^1]BF_4$, 0.1 mol dm^{-3} in $(CH_3)_2SO$ under Ar

T/K	T^{-1}/K^{-1}	$10^3\chi_M'$/c.g.s.u.*	$\mu_{eff.}/\mu_B$	T/K	T^{-1}/K^{-1}	$10^3\chi_M'$/c.g.s.u.*	$\mu_{eff.}/\mu_B$
83.0	0.0120	1.75	1.08	121.6	0.0082	1.51	1.21
85.0	0.0118	1.57	1.03	131.5	0.0076	1.48	1.25
87.4	0.0114	1.57	1.05	141.0	0.0071	1.43	1.27
89.5	0.0112	1.53	1.53	155.0	0.0065	1.35	1.30
92.4	0.0108	1.56	1.08	179.0	0.0056	1.25	1.34
99.0	0.0101	1.57	1.12	191.6	0.0052	1.23	1.37
105.0	0.0095	1.55	1.14	210.0	0.0048	1.06	1.33
115.0	0.0087	1.57	1.20				

* $\chi_M'_{,dia} = -0.0425$ c.g.s.u. ($[ZnL^1][BF_4]_2$ solution under Ar).

Table 4. Magnetochemical data for oxy-$[CuL^1]BF_4$, 0.1 mol dm^{-3} in $(CH_3)_2SO$

T/K	T^{-1}/K^{-1}	$10^3\chi_M''$/c.g.s.u.*	$\mu_{eff.}/\mu_B$	T/K	T^{-1}/K^{-1}	$10^3\chi_M''$/c.g.s.u.*	$\mu_{eff.}/\mu_B$
82.4	0.0121	3.69	1.56	141.4	0.0071	3.15	1.89
87.4	0.0114	3.32	1.52	153.9	0.0065	2.97	1.91
91.0	0.0110	3.39	1.57	166.9	0.0060	2.63	1.88
97.0	0.0103	3.56	1.66	182.0	0.0055	2.29	1.83
103.7	0.0096	3.65	1.74	199.5	0.0050	1.96	1.77
112.0	0.0089	3.55	1.78	220.2	0.0045	1.71	1.73
120.5	0.0083	3.39	1.81	250.0	0.0040	1.23	1.57
130.2	0.0077	3.31	1.86				

* $\chi_M''_{,dia.} = -0.0414$ c.g.s.u. ($[ZnL^1][BF_4]_2$ solution saturated with O_2).

Table 5. Magnetochemical 'difference' data for oxy-$[CuL^1]BF_4$, 0.1 mol dm^{-3} in $(CH_3)_2SO$

T/K	T^{-1}/K^{-1}	$10^3\chi_M$/c.g.s.u.*	$\mu_{eff.}/\mu_B$	T/K	T^{-1}/K^{-1}	$10^3\chi_M$/c.g.s.u.*	$\mu_{eff.}/\mu_B$
82.4	0.0121	2.11	1.18	130.2	0.0077	1.79	1.37
87.0	0.0115	1.82	1.13	141.4	0.0071	1.67	1.38
87.4	0.0114	1.75	1.11	153.9	0.0065	1.56	1.39
91.0	0.0110	1.82	1.15	166.9	0.0060	1.29	1.31
97.0	0.0103	1.99	1.24	182.0	0.0055	1.04	1.23
103.7	0.0096	2.10	1.32	199.5	0.0050	0.82	1.14
112.0	0.0089	1.98	1.33	220.2	0.0045	0.71	1.12
120.5	0.0083	1.88	1.35	250.0	0.0040	0.36	0.85

* $\chi_M = \chi_M'' - \chi_M'$ (see Tables 3 and 4).

tural data have confirmed the O_2 molecule to be co-ordinated to the iron centres of these species in a bent end-on fashion.[33,35]

Recently, resonance-Raman (r.R.) studies of several O_2-binding proteins (*e.g.* oxyhaemoglobin,[36] oxyhaemerythrin,[37] and oxyhaemocyanin[7]) and synthetic model compounds (*e.g.* $[\{Co(salen)_2L\}_2O_2]$ [38] [H_2salen = *N*,*N*′-ethylenebis(salicylideneiminate)] as well as the oxy-'picket fence' porphyrin [39]) have successfully determined the bond order of the ligated O_2 molecule and hence the electronic features of the metal–oxygen bonding scheme. In the case of oxyhaemocyanin, r.R. spectroscopy has been employed by Loehr and co-workers [2b,25,26] to define the copper–dioxygen interaction, as well as to identify the oxidation state of the copper centres. Oxyhaemocyanin has an intense absorption band at 345 nm (ε 10 000 dm^3 mol^{-1} cm^{-1}) and weaker bands around 570 nm (ε 500), and laser excitation in the visible region produced resonance enhancement of a Raman peak at 744 cm^{-1}. Based on an $^{18}O_2$ isotope shift to 704 cm^{-1}, this band has been conclusively assigned to the ν(O–O) mode.[38] This vibrational frequency is characteristic of the peroxide (O_2^{2-}) anion, and thus, the mode of the copper–dioxygen interaction seems to be well represented as Cu^{II}–O_2^{2-}–Cu^{II}.

In this work, r.R. spectra for the deoxy- and oxy-forms of $[CuL^1]^+$, the analogous copper(II) complex, and $[CuL^3]^+$, which is relatively unreactive towards oxygen, have been obtained by laser excitation in the visible wavelength region of the compounds' absorption spectra (see Experimental section). Using the 514.5-nm wavelength of an Ar^+/Kr^+ laser for excitation, the Raman spectra shown in Figure 7* were obtained for $[CuL^1]^+$ and $[CuL^3]^+$ at 77 K in frozen, deoxygenated solutions in CH_3CN.

Since these r.R. studies were undertaken mainly to characterize possible ν(O–O) frequencies, cycling between the deoxy-, oxy-, and redeoxy-forms of $[CuL^1]^+$ was exhaustively monitored. Figure 8 and Table 6 depict the results. Clearly, the r.R. spectrum of deoxy-$[CuL^1]^+$ is different from that of oxy-$[CuL^1]^{n+}$. Unfortunately, no Raman-active ν(O–O) frequency is obvious in the spectrum. In particular, the region of special interest for an O_2^{2-} (peroxide-like) stretching frequency would be *ca.* 700—800 cm^{-1}. However, this region of the spectrum for oxy-$[CuL^1]^{n+}$ is featureless. When the green oxygenated material is purged with N_2 the red, redeoxy-$[CuL^1]^{n+}$ solution

* Band positions (514.5 nm excitation): $[CuL^1]BF_4$ 1 002m, 1 038w, 1 183m, 1 330m, 1 373w, 1 409s, 1 465m, 1 557s, 1 588m, and 1 613m cm^{-1}; $[CuL^3]BF_4$ 726w, 753w, 811w, 1 002s, 1 123w, 1 150w, 1 182w, 1 223w, 1 247w, 1 314s, 1 327m, 1 409s, 1 513w, 1 557s, 1 588s, 1 611s, and 1 635s cm^{-1}.

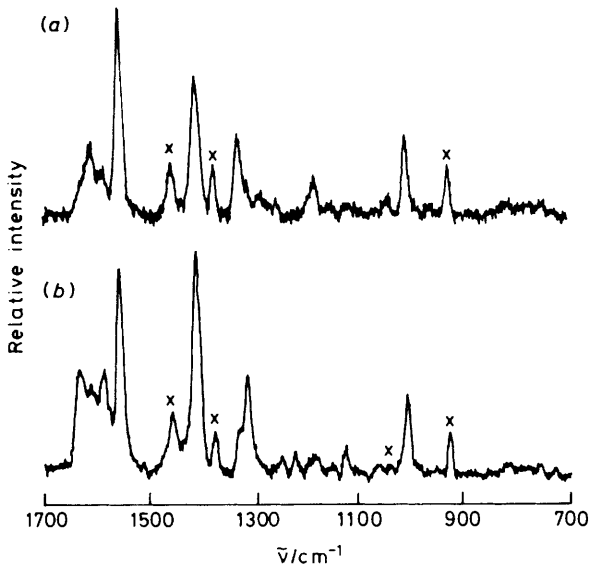

Figure 7. Resonance-Raman spectra of (*a*) deoxy-$[CuL^1]^+$ and (*b*) deoxy-$[CuL^3]^+$ obtained from frozen 0.1 mol dm^{-3} solutions in CH_3CN at 77 K using 514.5-nm excitation. Solvent bands are marked × under similar conditions, the solvent peak frequencies (and relative peak heights) are 774 (6), 924 (100), 1 043 (10), 1 378 (93), 1 424 (52), and 1 458 cm^{-1} (92). Crystals of complex (*a*) as the BF_4^- salt exhibit weak peaks at 1 038, 1 373, and 1 460 cm^{-1}, nearly coincident with solvent peaks

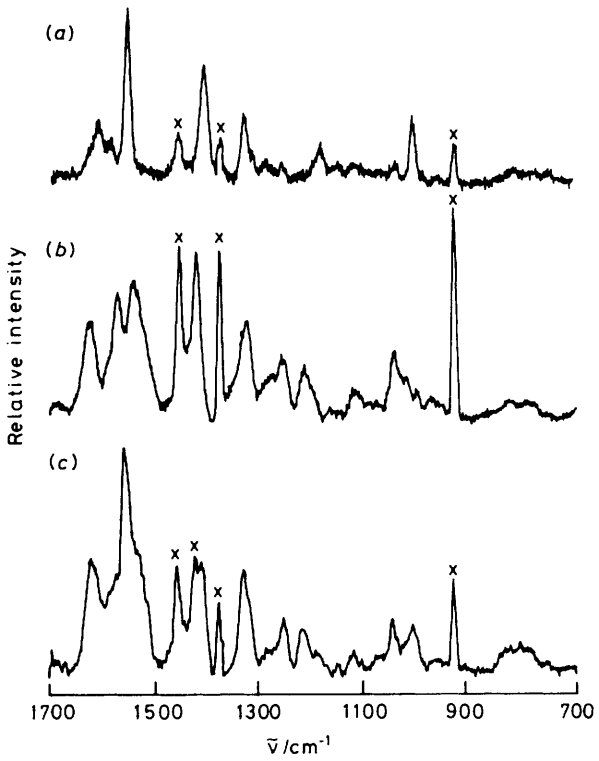

Figure 8. Resonance-Raman spectra obtained at 77 K for 0.1 mol dm^{-3} solutions in CH_3CN of (*a*) deoxygenated $[CuL^1]^+$ using 514.5-nm excitation, (*b*) oxygenated $[CuL^1]^{n+}$, and (*c*) redeoxygenated $[CuL^1]^{n+}$ using 457.9-nm excitation. Pure solvent bands are marked ×

is obtained, and the r.R. spectrum of a frozen aliquot of this contains vibrational bands for both deoxy- and oxy-$[CuL^1]^{n+}$. For example, the signals at 1 557 and 1 002 cm^{-1} in Figure 8(*a*) are absent in Figure 8(*b*) but are definitely present in Figure 8(*c*). Also in the spectrum of the redeoxy-material there are signals characteristic of the oxy-derivative, *i.e.* at 1 215 and 1 253 cm^{-1}. Thus, the r.R. data display the same partial reversibility of the O_2-cycling process that was first noticed in our earlier electronic absorption spectral studies.[1b]

In addition to reaction with $^{16}O_2$, $[CuL^1]^+$ has been oxygenated with $^{18}O_2$ and its r.R. spectrum obtained. Figure 9 and Table 7 illustrate the comparative spectral data obtained from these $^{16}O_2$ and $^{18}O_2$ experiments, as well as data for the analogous copper(II) complex. Since the $^{16}O_2$ and $^{18}O_2$ oxy-forms of $[CuL^1]^{n+}$ exhibit essentially identical spectra, no isotope effect is revealed. Here it is important to emphasize that the absence of an assignable ν(O–O) from these initial isotope-labelling studies does not necessarily mean that oxy-$[CuL^1]^{n+}$ does not contain a $Cu–O_2$ or $Cu–O_2–Cu$ unit, since detection of ν(O–O) is dependent on the experimental and resonance conditions. However, it is clear from Figure 9 that the spectrum of the analogous copper(II) compound differs substantially from that of the oxygenated copper(I) species. Most noticeably, the intensities and numbers of peaks in the 1 100—1 700 cm^{-1} region for the oxygenated copper(I) samples are different in the two compounds. Thus, the spectrum and nature of oxygenated $[CuL^1]^{n+}$ is definitely different from that of $[CuL^1]^{2+}$.

While the r.R. experiments involving laser excitation in the visible region of the absorption spectrum have yielded some information concerning the oxygenation of $[CuL^1]^+$, u.v. excitation has offered additional insight into the copper–dioxygen reaction. R.R. spectra obtained at room temperature for $[^{16}O_2]$oxy-$[CuL^1]^{n+}$ and $[CuL^1]^{2+}$, and in CH_3CN from excitation at 363.8 and 413.1 nm, yielded the data in Table 8. Comparison of the spectral data for $[CuL^1]^{2+}$ obtained by

Table 6. Resonance-Raman spectral data [a] for the deoxy-, oxy-, and redeoxy-forms of $[CuL^1]BF_4$, 0.1 mol dm^{-3} in CH_3CN

deoxy-$[CuL^1]^+$ (514.5 nm) [b]	1 002m, 1 038w, 1 183m, 1 330m, 1 373w, 1 409s, 1 465m, 1 557s, 1 588m, 1 613m
$[^{16}O_2]$Oxy-$[CuL^1]^{n+}$ (457.9 nm) [b]	821w, 1 013w, 1 116w, 1 163w, 1 212m, 1 254m, 1 275m, 1 321s, 1 540s, 1 573s, 1 623s
redeoxy-$[CuL^1]^{n+}$ (457.9 nm) [b]	819w, 1 002m, 1 011m, 1 068w, 1 117m, 1 148w, 1 186w, 1 215m, 1 253m, 1 284w, 1 316 (sh), 1 329s, 1 413s, 1 538 (sh), 1 557s, 1 610 (sh), 1 622s

[a] s = Strong, m = medium, w = weak, and (sh) = shoulder. [b] Excitation wavelength.

visible and u.v. excitation reveals several points of interest. Some r.R. signals appearing from visible excitation are not present when the u.v. laser lines are used for excitation. Thus, selective resonance enhancement of certain Raman peaks is observed when u.v. and violet excitation is employed. Certain other modes, which are observed with visible excitation, apparently are not enhanced in the violet of u.v. regions. While resonance enhancement could in principle result from the electronic transitions in the visible region, the Raman bands observed in visible excitation are fairly weak in intensity considering the high concentrations of solute (0.1 mol dm^{-3}). Thus, these lines are probably normal (non-resonant) Raman peaks, or else only weakly preresonance-enhanced ones. The resonance enhancement of Raman peaks in the u.v. experiment most likely originates from u.v. electronic trans-

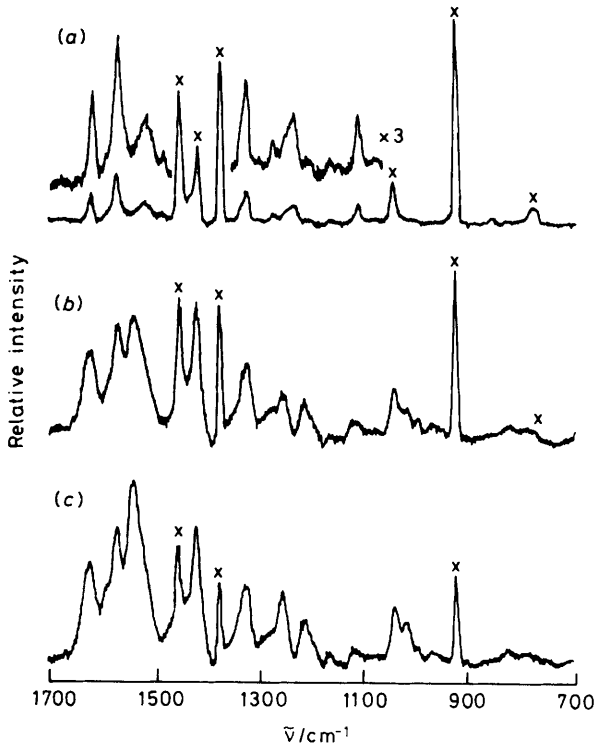

Figure 9. Resonance-Raman spectra obtained at 77 K for 0.1 mol dm^{-3} solutions in CH_3CN of (*a*) $[CuL^1]^{2+}$ using 514.5-nm excitation (the spectral contributions of the solvent, marked ×, predominate over those of the complex under these conditions), (*b*) $^{16}O_2$-oxygenated $[CuL^1]^{n+}$, and (*c*) $^{18}O_2$-oxygenated $[CuL^1]^{n+}$ using 457.9-nm excitation

itions involving ring-localized $\pi \rightarrow \pi^*$ states, resulting in enhancement of vibrational modes of the 'rings;' the fact that the signal intensities vary relative to one another as different u.v. excitation lines are employed (see Table 8) is further support for a u.v.-based selective enhancement.

No r.R. spectrum of the deoxy-$[CuL^1]^+$ species was obtained for any of the u.v. or violet laser lines. The reason for this is unclear. In a series of concentration-dependent experiments using u.v. excitation no solute spectrum was observed under any conditions ranging from negligible attenuation of solvent peaks by the electronic absorption (ε 1 500 dm^3 mol^{-1} cm^{-1}) of the solute to total attenuation of the solvent peaks by self-absorption. This observation is virtually unprecedented for a molecule having strong $\pi \rightarrow \pi^*$ transitions in the near-u.v. Interference (anti-resonance) effects appear to be precluded because a range of laser wavelengths (413.1—363.8 nm) yields the same results. Apparently, the displacement of the excited-state potential surface is extremely small, resulting in negligible Franck–Condon r.R. enhancement in this complex.

The $[^{16}O_2]$oxy-$[CuL^1]^{n+}$ derivative yields the r.R. spectrum detailed in Table 8. As with the visible excitation study, the u.v. experiment also revealed no ν(O–O) band. Apparently, no significant ligand (π system) structural changes occur during oxygenation of the copper(I) species since the 1 300—1 600 cm^{-1} region of the r.R. spectrum is virtually identical, with respect to band position, for $[CuL^1]^{2+}$ and $[^{16}O_2]$oxy-$[CuL^1]^{n+}$. In addition, most of the resonance enhancement results from the transition at 300 nm in the absorption spectrum of $[CuL^1]^{2+}$. Since $[^{16}O_2]$oxy-$[CuL^1]^{n+}$ has no such absorption in this region, it likewise has a more sparse r.R. spectrum. Comparison of this 1 300—1 600 cm^{-1} region for these two copper samples reveals noticeable differences in signal intensities. Thus, the species yielding the copper(II) r.R. spectrum is not identical to that which gives the oxy-copper r.R. spectrum, as was also concluded above from the visible-excitation experiments.

Finally, $[CuL^2]^{2+}$ and $[CuL^2]^+$ were also investigated for comparative purposes, but unfortunately deoxy-$[CuL^2]^+$ and $[^{16}O_2]$oxy-$[CuL^2]^{n+}$ were found to luminesce under u.v. laser illumination. The intense fluorescence spectrum masked the Raman scattering. However, an r.R. spectrum was easily obtained for the analogous copper(II) complex, * and the spectral data are very similar to data for $[CuL^1]^{2+}$ with the small observed differences attributable to the somewhat different ligand framework.

Table 7. Resonance-Raman spectral data [a] for $[CuL^1]^{2+}$ and the $^{16}O_2$- and $^{18}O_2$-oxygenated forms of $[CuL^1]^+$

$[CuL^1]^{2+}$ (514.5 nm) [b]	822w, 853w, 1 015m, 1 110m, 1 164w, 1 202w, 1 234m, 1 274w, 1 325s, 1 336 (sh), 1 521s, 1 577s, 1 626s
$[^{16}O_2]$oxy-$[CuL^1]^{n+}$ (457.9 nm)	821w, 1 013w, 1 039m, 1 116w, 1 163w, 1 212m, 1 254m, 1 275w, 1 325s, 1 422s, 1 544s, 1 573s, 1 623s
$[^{18}O_2]$oxy-$[CuL^1]^{n+}$ (457.9 nm)	822w, 1 015m, 1 039m, 1 116w, 1 164w, 1 212m, 1 253m, 1 275w, 1 325m, 1 421s, 1 542s, 1 575s, 1 595 (sh), 1 626s

[a] s = Strong, m = medium, w = weak, and (sh) = shoulder. [b] Excitation wavelength.

Table 8. Resonance-Raman spectral data * for (*a*) $[CuL^1][BF_4]_2$ (13.2 mmol dm^{-3}) and (*b*) $[^{16}O_2]$oxy-$[CuL^1]^{n+}$ (4.35 mmol dm^{-3}) in CH_3CN at 295 K

Excitation wavelength (nm)	(*a*) 413.1, 363.8; (*b*) 363.8
Signal position (cm^{-1})	(*a*) 794w, 1 072w, 1 103w, 1 115m, 1 160w, 1 213w, 1 250s, 1 258s, 1 307s, 1 322w, 1 332w, 1 472m, 1 573m, 1 580m, 1 600w, 1 622w, 1 256w, 1 309w, 1 323m, 1 576m, 1 590 (sh), 1 621m; (*b*) 1 332w, 1 572m, 1 595m, 1 620w

* s = Strong, m = medium, and w = weak.

Conclusions

Through the systematic variation of ligand structure, a family of imidazole-bearing, O_2-active copper(I) complexes has been synthesized and their reversible reaction with O_2 studied. The analogous copper(II) compounds have been examined by electrochemical techniques and a correlation observed: the more positive the $E_{\frac{1}{2}}$ for the $Cu^{II} \rightleftharpoons Cu^{I}$ couple, the greater the stability of the copper(I) species, generated at the electrode surface, and the lower (and slower) is the reactivity of the copper(I) centre towards O_2 in a reversible manner. These

* R.R. data for $[CuL^2]^{2+}$ (0.091 mol dm^3 in CH_3CN) at 295 K with 406.7-nm excitation: 1 104w, 1 120m, 1 162w, 1 188w, 1 216w, 1 248s, 1 256s, 1 314s, 1 332m, 1 352w, 1 472m, 1 580s, and 1 600w cm^{-1}.

particular copper(I) complexes have also been studied in order to examine the role, if any, of the imidazole-nitrogen proton in the reversible oxygenation of the parent $[CuL^1]^+$. The 'protonless' $[CuL^4]^+$ species reacts with O_2 (O_2 : Cu = 1 : 2) in a similar fashion to $[CuL^1]^+$. Clearly the oxygenation process for $[CuL^4]^+$ cannot involve imidazole-nitrogen protons. Possibly, the mechanisms of oxygenation for these two copper(I) complexes differ, but it seems unlikely given the available experimental data. Furthermore, the spectroscopic, electrochemical, and magnetochemical data presented provide some additional support for the previously proposed binuclear $LCu^{II}-O_2^{2-}-Cu^{II}L$ structure for the oxygenated copper species.[1b] Although the resonance-Raman experiments have not yet yielded a ν(O–O) for oxy-$[CuL^1]^{n+}$ the relative r.R. peak intensities demonstrate that oxygenated $[CuL^1]^{n+}$ differs from oxidized $[CuL^1]^{2+}$. Furthermore, the similarities of the r.R. frequencies observed for the copper(I) and oxygenated copper(I) species suggest that no large perturbation (*e.g.* oxidation) of the organic ligand moiety occurs, at least during the initial oxydeoxy cycling. Final proof as to whether these copper complexes are indeed simple O_2 carriers may lie in furtner r.R. work under different conditions or with the other copper(I) species, or preferably in the growth of a single crystal of an oxygenated species for detailed structural characterization. Both fronts are being intensively pursued.

Acknowledgements

L. J. W. is grateful to The Robert A. Welch Foundation and the U.S. National Institutes of Health (N.I.H.) for support, and T. M. L. and W. H. W. also acknowledge support by the N.I.H. Finally, we thank Dr. Michael F. Tweedle for assistance in obtaining the magnetochemical results.

References

1 (*a*) M. G. Simmons and L. J. Wilson, *J. Chem. Soc., Chem. Commun.*, 1978, 634; (*b*) M. G. Simmons, C. L. Merrill, L. J. Wilson, L. A. Bottomley, and K. M. Kadish, *J. Chem. Soc., Dalton Trans.*, 1980, 1827.
2 (*a*) E. I. Solomon, D. M. Dooley, R. Wang, H. B. Gray, M. Cerdonio, F. Mogno, and G. I. Romani, *J. Am. Chem. Soc.*, 1976, **98**, 1029; (*b*) T. B. Freedman, J. S. Loehr, and T. M. Loehr, *ibid.*, p. 2809.
3 B. A. Averill, personal communication.
4 P. Hemmerich and C. Sigwart, *Experientia*, 1963, **19**, 488.
5 (*a*) W. W. Umbreit, R. H. Burris, and J. F. Stauffer, in 'Manometric Techniques,' 4th edn., Burgess, Minneapolis, 1964; (*b*) A. G. Zwart, *Biochem. Biophys. Acta*, 1952, **9**, 104.
6 M. F. Tweedle and L. J. Wilson, *Rev. Sci. Instrum.*, 1978, **49**, 1001.
7 M. F. Tweedle, L. J. Wilson, L. Garcia-Iniguez, G. T. Babocck, and G. Palmer, *J. Biol. Chem.*, 1978, **253**, 8065.
8 T. M. Loehr, W. E. Keyes, and P. A. Pincus, *Anal. Biochem.*, 1979, **96**, 456.
9 B-M. Sjöberg, T. M. Loehr, and J. Sanders-Loehr, *Biochemistry*, 1982, **21**, 96.
10 D. F. Shriver and J. B. R. Dunn, *Appl. Spectrosc.*, 1974, **28**, 319.
11 J. D. Korp, I. Bernal, C. L. Merrill, and L. J. Wilson, *J. Chem. Soc., Dalton Trans.*, 1981, 1951.
12 M. Pasquali, G. Marini, C. Floriani, A. Gaetani-Manfredotti, and C. Guastini, *Inorg. Chem.*, 1980, **19**, 2525.
13 C. Mealli, C. S. Arcus, J. L. Wilkinson, T. J. Marks, and J. A. Ibers, *J. Am. Chem. Soc.*, 1976, **98**, 711.
14 R. R. Gagné, R. S. Gall, G. C. Lisensky, R. E. Marsh, and L. M. Speltz, *Inorg. Chem.*, 1979, **18**, 771; R. R. Gagné, J. L. Allison, and D. M. Ingle, *ibid.*, p. 2767.
15 D. Van der Helm, A. F. Nicholas, and C. G. Fisher, *Acta Crystallogr., Sect. B*, 1970, **26**, 1172.
16 S. E. V. Phillips and B. P. Schoenborn, *Nature (London)*, 1981, **292**, 81.
17 M. G. Burnett, V. McKee, and S. M. Nelson, *J. Chem. Soc., Chem. Commun.*, 1980, 599.
18 K. Hofmann, in 'Imidazole and Its Derivatives,' Interscience, New York, 1953, ch. 8, p. 254.
19 H. H. Wasserman, K. Stiller, and M. B. Floyd, *Tetrahedron Lett.*, 1968, 3277.
20 C. S. Foote, E. R. Peterson, and H. S. Ryang, presented at the Seventh Meeting of the American Society of Photochemists, Monterey, June, 1978.
21 T. Matsuura and I. Saito, *Chem. Commun.*, 1967, 693.
22 L. Weil, S. James, and A. R. Buchert, *Arch. Biochem. Biophys.*, 1953, **46**, 266.
23 G. Jori, B. Salvato, and L. Tallandini, in 'Structure and Function of Haemocyanin,' ed. J. V. Bannister, Springer, Berlin, 1977, pp. 156—163.
24 R. Barbucci, A. Mastroianni, and M. J. M. Campbell, *Inorg. Chim. Acta*, 1978, **27**, 109.
25 J. S. Loehr, T. B. Freedman, and T. M. Loehr, *Biochem. Biophys. Res. Commun.*, 1974, **56**, 510.
26 T. J. Thamann, J. S. Loehr, and T. M. Loehr, *J. Am. Chem. Soc.*, 1977, **99**, 4187.
27 J. A. Larrabee, T. G. Spiro, N. S. Ferris, W. H. Woodruff, W. A. Maltese, and M. S. Kerr, *J. Am. Chem. Soc.*, 1977, **99**, 1979.
28 J. A. Larrabee and T. G. Spiro, *J. Am. Chem. Soc.*, 1980, **102**, 4217.
29 J. M. Brown, L. Powers, B. Kincaid, J. A. Larrabee, and T. G. Spiro, *J. Am. Chem. Soc.*, 1980, **102**, 4210.
30 R. S. Himmelwright, N. C. Eickman, and E. I. Solomon, *J. Am. Chem. Soc.*, 1979, **101**, 1576; R. S. Himmelwright, N. C. Eickman, C. D. LuBien, and E. I. Solomon, *ibid.*, 1980, **102**, 5378; N. C. Eickman, R. S. Himmelwright, and E. I. Solomon, *Proc. Natl. Acad. Sci. USA*, 1979, **76**, 2094.
31 V. McKee, J. V. Dagdigian, R. Bau, and C. Reed, *J. Am. Chem. Soc.*, 1981, **103**, 7000.
32 Kino, S. Suzuki, W. Mori, and A. Nakahara, *Inorg. Chim. Acta*, 1981, **56**, L33.
33 J. P. Collman, R. R. Gagné, C. A. Reed, T. R. Halbert, G. Lang, and W. T. Robinson, *J. Am. Chem. Soc.*, 1978, **97**, 1427; J. P. Collman, J. I. Brauman, T. P. Collins, B. Iverson, and J. L. Sessler, *ibid.*, 1981, **103**, 2450; J. P. Collman, *Acc. Chem. Res.*, 1977, **10**, 265.
34 J. P. Collman, J. I. Brauman, T. R. Halbert, and K. S. Suslick, *Proc. Natl. Acad. Sci. USA*, 1976, **73**, 3333.
35 B. Shaanan, *Nature (London)*, 1982, **296**, 683.
36 T. G. Spiro and T. C. Strekas, *Proc. Natl. Acad. Sci. USA*, 1972, **69**, 2622.
37 D. M. Kurtz, jun., D. F. Shriver, and I. M. Klotz, *Coord. Chem. Rev.*, 1977, **24**, 145.
38 E. M. Nour and R. E. Hester, *J. Mol. Struct.*, 1980, **62**, 77; M. Suzuki, T. Ishiguro, M. Kozuka, and K. Nakamoto, *Inorg. Chem.*, 1981, **20**, 1993.
39 M. A. Walters, T. G. Spiro, K. S. Suslick, and J. P. Collman, *J. Am. Chem. Soc.*, 1980, **102**, 6857.

Received 10*th August* 1983; *Paper* 3/1403